ISSN 0869-5938, Stratigraphy and Geological Correlation, 2020, Vol. 28, No. 4, pp. 343–364. © Pleiades Publishing, Ltd., 2020.
Russian Text © The Author(s), 2020, published in Stratigrafiya, Geologicheskaya Korrelyatsiya, 2020, Vol. 28, No. 3, pp. 3–26.

Carbonate Deposits of Eastern Sarmatia (Early Precambrian Ignateevo Formation, Kursk Block): Sedimentation Conditions and Paleocontinental Correlations

K. A. Savko[a], *, A. B. Kuznetsov[b], and M. Yu. Ovchinnikova[a]

[a] *Voronezh State University, Voronezh, Russia*

[b] *Institute of Precambrian Geology and Geochronology, Russian Academy of Sciences, St. Petersburg, Russia*

**e-mail: ksavko@geol.vsu.ru*

Received May 8, 2019; revised July 12, 2019; accepted November 20, 2019

Abstract—The Neoarchean–Early Paleoproterozoic section of the Eastern Sarmatia Kursk Block contains different formations: terrigenous-carbonate (Ignateevo Formation), terrigenous (Stoilo Formation), and banded iron (Korobki Formation). The Kursk Block sequences have obvious similarities to the coeval terrigenous-carbonaceous-ferriferous formations of the Kaapvaal and Pilbara cratons. The Ignateevo Formation dolomites are correlated with the Campbellrand–Malmani and Wittenoom–Carawine carbonate platforms. Carbonate rocks of all three cratons are silicified and show no evidence of clastic contamination. They are characterized by low Sr concentrations and are enriched in Fe and Mn. The REE distribution in carbonate rocks is characteristic of Neoarchean marine sediments: flat profiles on spider diagrams, positive La anomalies, absence of Ce anomaly, and increased Y/Ho ratios relative to the chondrite value. The values of $\delta^{13}C$ (0.3–0.9‰ PDB) and $\delta^{18}O$ (–10.1 to –13.0‰ PDB) in the Ignateevo Formation dolomites fall within the range of the Late Archean and Early Paleoproterozoic marine carbonate sediments. The $^{87}Sr/^{86}Sr$ ratio in the Ignateevo Formation dolomites (0.7101–0.7195) is higher than that in the Neoarchean marine carbonates, which implies either isolation of the paleobasin or disturbance of the Rb–Sr isotope systems during metamorphism. The Ignateevo Formation dolomites and calc-silicate rocks (intensively silicified dolomites) are closest in their isotope-geochemical characteristics to shallow-water dolomites of the Campbellrand–Malmani Platform (South Africa). Probably, the Ignateevo Formation dolomites and partly the formations composing the Campbellrand–Malmani Platform formed in the most isolated part of the paleobasin, which facilitated to their complete dolomitization and partial silicification.

Keywords: Vaalbara, Kaapvaal, Pilbara, Sarmatia, carbonate rocks, dolomites, correlation of geological sections

DOI: 10.1134/S0869593820030107

INTRODUCTION

Archean sedimentary formations serve as the basis for paleocontinental correlations of the early Earth. The two largest Early Precambrian cratons, Pilbara and Kaapvaal, contain thick strata of banded iron formations (BIFs) formed at the the Archean–Proterozoic boundary ca. 2.5 Ga. An important feature of the BIFs is that they occur on Neoarchean deposits of carbonate platforms. In the Kaapvaal craton, the Transvaal iron-ore formations occur on the shallow-water Campbellrand–Malmani carbonates (Klein and Beukes, 1989; Beukes et al., 1990). In the Pilbara craton, the shallow-water Wittenoom–Carawine dolomites underlie BIFs of the Hamersley Group (Jahn and Simonson, 1995). The mentioned carbonate platforms formed in the time interval of 2.6–2.5 Ga (Sumner and Beukes, 2006). The correlation of the Archean and Paleoproterozoic sediments of the Pilbara and Kaapvaal cratons gave grounds to the idea that they belonged to the united Vaalbara supercontinent (Cheney, 1996; Nelson et al., 1999; Beukes and Gutzmer, 2008).

The sequence of geological events established in the deposits of the Kursk Block in the time interval of 2.8–2.2 Ga (Figs. 1a, 1b) allowed us to suggest that Eastern Sarmatia belonged to the Vaalbara supercontinent (Savko et al., 2017). Carbonate deposits of the Ignateevo Formation, underlying the Paleoproterozoic BIF in the Kursk Block, are the key evidence in argumentation for this conclusion (Fig. 1c). This determines the need for a detailed study of Early Precambrian carbonate rocks in the Kursk Block, in order to justify the paleogeodynamic position of Eastern Sarmatia as an integral part of the Vaalbara supercontinent.

The purpose of this publication is to present the structure of the Archean–Paleoproterozoic sedimentary section of the Kursk Block, to obtain new data on the mineral and isotope-geochemical composition of the Ignateevo Formation dolomites, and, on the basis of these data, to assess the sedimentation conditions of

carbonate deposits at the Archean–Paleoproterozoic boundary and to perform paleocontinental correlations with the Campbellrand–Malmani carbonate platform of the Kaapvaal craton and the Wittenoom–Carawine carbonate platform of the Pilbara craton.

GEOLOGICAL OVERVIEW

The Archean basement of the Kursk Block is composed of granite gneisses of the Oboyan complex and tonalite-trondhjemite-granodiorites (TTGs) of the Saltykovo complex of about 3 Ga in age (Savko et al., 2018), among which there are fragments of greenstone areas composed mainly of metabasites of the Mikhailovka Series (Fig. 1c). High-temperature metamorphism ended the formation cycle of Sarmatia's ancient Mesoarchean basement ca. 2.8 Ga (Savko et al., 2018). Paleoproterozoic terrigenous-chemogenic sedimentary rocks of the Kursk Series, which includes the Ignateevo, Stoilo, and Korobki Formations, occur on the Mesoarchean basement. They have an aggregated thickness of over 1.2 km and a broad spatial distribution; additionally, they were not eroded within the continental riftogenic structures nucleated in the mid-Paleoproterozoic ca. 2.2 Ga on the Archean basement (Savko et al., 2017).

The largest riftogenic structures of the Kursk Block are the Belgorod–Mikhailovka and Tim–Yastrebovka ones (Fig. 1b). These objects demonstrate different structures of their Paleoproterozoic sedimentary sections. Potassium rhyolites of 2610 Ma in age occur at the base of the terrigenous-chemogenic sequence in the Tim–Yastrebovka structure (Savko et al., 2019). The rhyolite weathering crust is overlain by basal quartz conglomerates of the Paleoproterozoic Stoilo Formation. These deposits are a geochronological reference marking the hiatus and the initiation of the marine basin, where Paleoproterozoic BIFs formed later (Savko et al., 2015). Up the section, metaconglomerates are replaced with quartz metasandstones and aluminous shales of the Stoilo Formation, conformably superimposed by rocks of the Korobki BIF (Fig. 1c).

In the Mikhailovka riftogenic structure, metaconglomerates of the Ignateevo Formation occur at the bottom of the metasedimentary section; they rest erosively on the Mesoarchean TTG and Archean metabasites of the Mikhailovka Series (Figs. 1c, 2). Metaconglomerates are replaced above with polymictic gravelites and metasandstones. The Ignateevo Formation is topped by a dolomite stratum up to 160 m thick. Arkosic metasandstones, intercalated with shales and carbonate rocks of the Stoilo Formation, conformably occur on dolomites. Up the section, metasandstones change from arkosic to feldspar-quartz and quartz ones. In marginal parts of the structure, intercalations of quartz metagravelites and metaconglomerates are found. The upper part of the Stoilo Formation in the Mikhailovka structure is represented predominantly by carbonaceous and aluminous shales. Above this, conformably resting on the Stoilo Formation deposits, rocks of the Korobki BIF occur.

In all structures of Eastern Sarmatia, a thick sedimentary sequence of the Kursk Series, occurring on the Archean basement, underwent folding and metamorphism ca. 2.07 Ga during the collision between the Sarmatia and Volgo-Uralia megablocks (Savko et al., 2018). The parameters of that metamorphism, as inferred from mineral parageneses from overlying metapelites of the Stoilo Formation and from rocks of the Korobki BIF, are 370–520°C and 2–3 kbar (Savko and Poskryakova, 2003a, 2003b). Tectonic stress resulting from the collision was directed eastward (in present-day coordinates), formed a series of thrusts, and caused an intense folding in the eastern sides of the Paleoproterozoic synforms (Savko et al., 2018). This explains the "overturned occurrence" of metasedimentary rocks, which is observed only in the eastern side of the Mikhailovka structure (according to the cores recovered from Boreholes 3748, 3759, and 3785), where Archean rocks were thrusted over the Paleoproterozoic ones and underwent complex folding (overturned folds in Fig. 2). Paleoproterozoic sediments are fragmented here, and small fragments fall within the zone where the Mesoarchean granite-gneiss basement developed (Fig. 1c).

Archean rocks underlying the Ignateevo Formation were recovered in Boreholes 3573, 3748, 3759, and 3785 (Fig. 2). In Borehole 3573, polymictic conglomerates of the Ignateevo Formation are underlain by metabasites of the Neoarchean Aleksandrovka Formation; down the section, Mesoarchean trondhjemites of the Saltykovo complex are recovered. In some boreholes (3729, 3748, 3759, and 3785), an overturned occurrence of rocks is observed, as a result of which the Ignateevo Formation deposits are overlain by migmatized gneisses of the Oboyan complex and by TTGs and are underlain by quartzite sandstones of the Stoilo Formation (Borehole 3764; Fig. 2). In Borehole 3748, the weathering crust composed of biotite plagiogneisses of the Oboyan complex was identified. In the western side of the Mikhailovka structure, carbonate deposits of the Ignateevo Formation occur in the

Fig. 1. (a) Scheme of the segments of the East European craton after (Gorbatschev and Bogdanova, 1993), (b) schematic structural map of Sarmatia for the Voronezh crystalline massif, and (c) schematic geologic map of the Mikhailovka structure. Legend: (1) Oboyan complex (AR_1ob); (2) Mikhailovka Series (AR_2mh); (3) Ignateevo Formation (PR_1ig); (4) Stoilo Formation (PR_1st); (5) Korobkovo Formation (PR_1kr); (6) Rogovoe Formation (PR_1rg); (7) Kurbakinskaya Formation (PR_1kb); (8) Zolotukhino complex (νPR_1z); (9) Stoilo-Nikolaevka complex ($\gamma\delta PR_1$sn); (10) Atamanskii complex (γPR_1at); (11) ages of igneous bodies and metamorphic events, in Ma; (12) ferriferous quartzites; (13) shales; (14) dolomites; (15) metaconglomerates; (16) metasandstones; (17) metabasites; (18) metarhyolites; (*19*) granitoids.

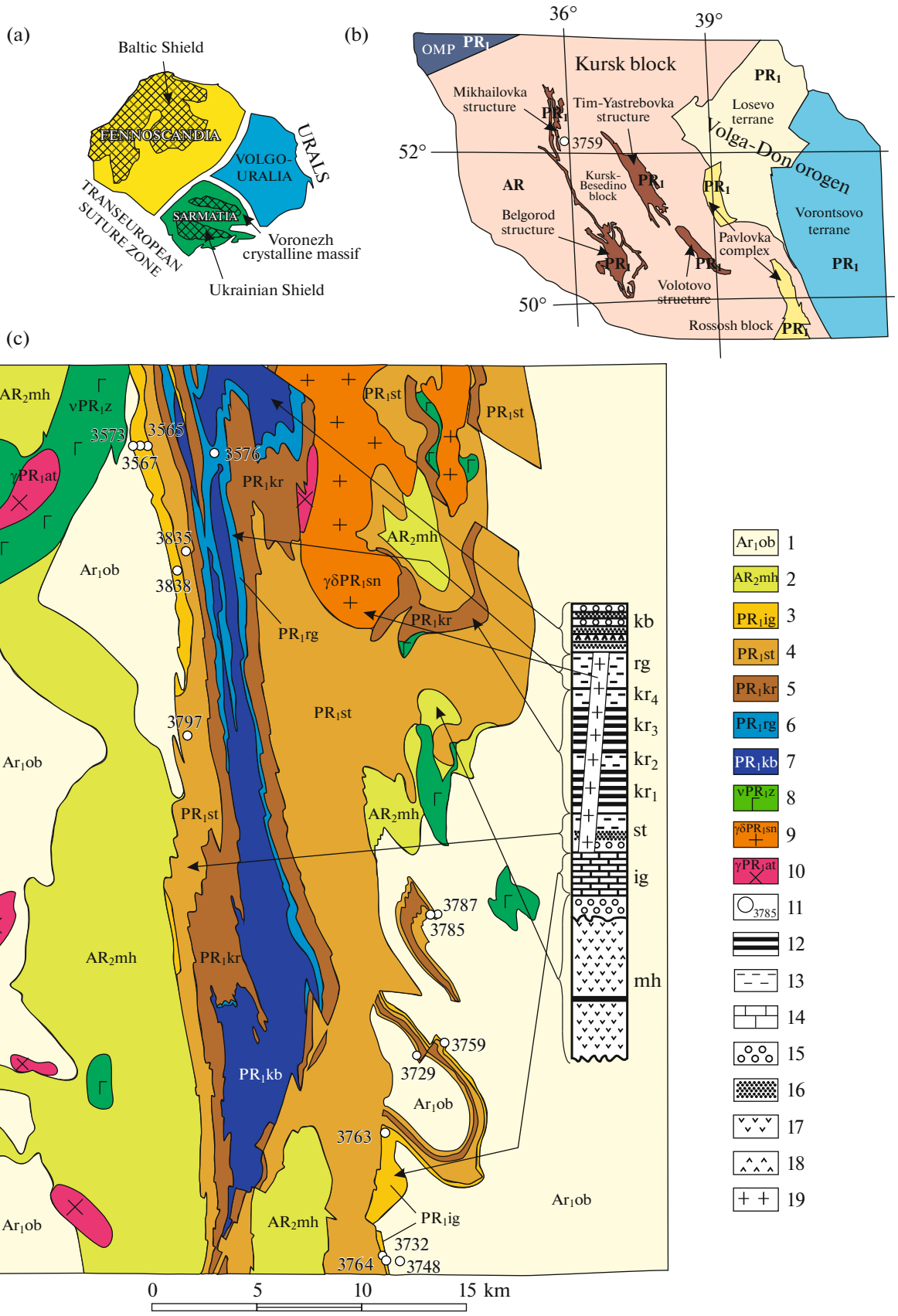
(a)
Baltic Shield
FENNOSCANDIA
VOLGO-URALIA
URALS
SARMATIA
TRANSEUROPEAN SUTURE ZONE
Voronezh crystalline massif
Ukrainian Shield
(b)
36°
39°
52°
50°
OMP PR1
Kursk block
PR1
Mikhailovka structure
Tim-Yastrebovka structure
Losevo terrane
3759
Volga-Don orogen
AR
Kursk-Besedino block
Belgorod structure
Pavlovka complex
Vorontsovo terrane
Volotovo structure
Rossosh block
(c)
AR2mh
vPR1z
3573
3565
3567
3576
γPR1at
PR1kr
PR1st
3835
3838
Ar1ob
γδPR1sn
PR1rg
3797
PR1kb
3787
3785
3759
3729
3763
PR1ig
3732
3764
3748
kb
rg
kr4
kr3
kr2
kr1
st
ig
mh
0 5 10 15 km
1 Ar1ob
2 AR2mh
3 PR1ig
4 PR1st
5 PR1kr
6 PR1rg
7 PR1kb
8 vPR1z
9 γδPR1sn
10 γPR1at
11 3785
12
13
14
15
16
17
18
19

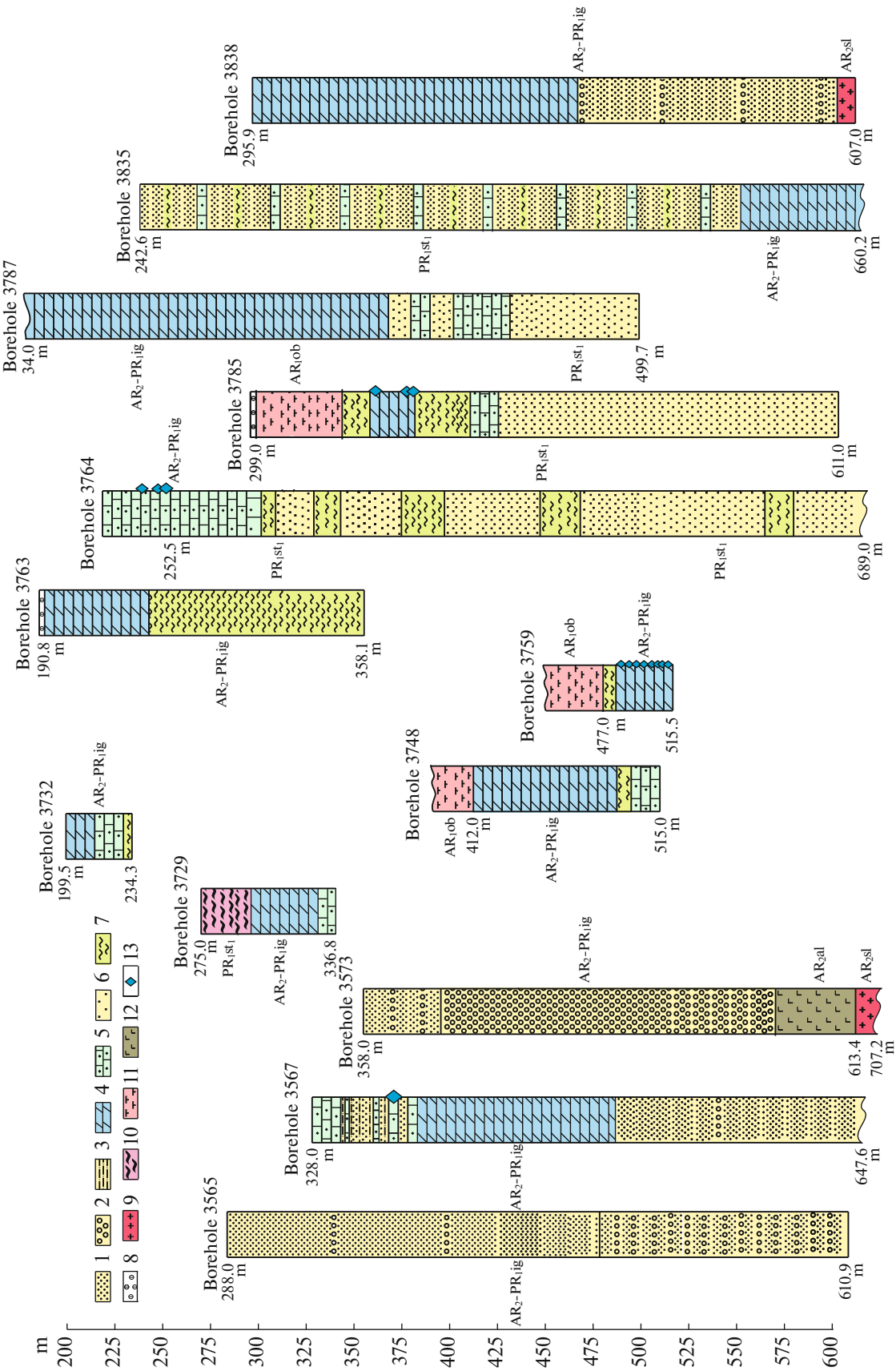

Fig. 2. Stratigraphic columns of boreholes that uncovered the Ignateevo Formation within the limits of the Mikhailovka structure. Legend: (1) metasandstones; (2) metaconglomerates; (3) metasiltstones; (4) dolomites; (5) calc–silicate rocks; (6) quartzite sandstone; (7) shales; (8) weathering crust; (9) granitoids of the TTG association; (10) migmatites; (11) gneisses; (12) metabasites; (13) sampling points. Stratigraphic units: AR_1ob, Oboyan complex; AR_2sl, Saltykovo complex; AR_2al, Aleksandrovka Formation, Mikhailovka Series (AR_2mh); $AR_2–PR_1ig$, Ignateevo Formation; PR_1st, Stoilo Formation.

normal position (Boreholes 3573, 3835, and 3838) on the Archean basement and are overlain by a sequence of metasandstones (sometimes gravel-bearing) interbedding with shales and carbonate rocks of the Stoilo Formation.

Carbonate rocks of the Ignateevo Formation do not contain stromatolithic and microphytolithic fossils and carry no clear structural features for determining deposition environments because of metamorphic recrystallization ca. 2.07 Ga (Savko et al., 2018).

STRUCTURE OF THE IGNATEEVO FORMATION

The Ignateevo Formation up to 800 m thick has a two-member structure. The lower terrigenous member (110–680 m) consists of polymictic metaconglomerates, metagravelites, and metasandstones (Fig. 2). The upper carbonate member (up to 160 m) is represented by dolomites and calc-silicate rocks (Fig. 2).

The lower terrigenous part of the formation has at its bottom a metaconglomerate member of about 150 m thick (Fig. 2, Boreholes 3565 and 3573). Polymictic metaconglomerates are gray (or dark gray with a greenish tincture) and sometimes show signs of weakly expressed schistosity and blastopsephitic structure. The pebble content is up to 40–50%, sometimes up to 60–80%. Cement is represented by metasandstones consisting of quartz (20–60%), plagioclase (10–45%), fine-scaled muscovite (5–30%), biotite (5–20%), chlorite (0–25%), and carbonate (0–15%); microcline is sometimes noted. Accessory minerals are sphene, zircon, tourmaline, sulfides, and hematite/magnetite. Large fragments are represented by schistose metabasites, TTGs, quartzites, and microcline granites.

Up the section, metaconglomerates gradually change to metagravelites and metasandstones intercalated with conglomerates (Boreholes 3565, 3573, 3799, and 3838). The rocks are gray with a greenish tint and possess blastopsephitic and blastopsammitic textures and an indistinctly schistose structure. Pebbles in metaconglomerates and fragments in metagravelites are represented with TTGs, metabasites, shales, and quartzites. The thickness of the member is 190 m.

Metagravelites are gradually replaced with polymictic medium- and coarse-grained gray sandstones possessing blastopsammitic texture and indistinctly banded structure (Boreholes 3565, 3567, and 3838). They consist of quartz (40–50%), plagioclase (10–30%), microcline (5–10%), and fine-scaled muscovite (20–30%). The thickness of the metasandstone member is about 240 m.

Carbonate rocks (up to 160 m thick) occur at the top of the Ignateevo Formation section and rest conformably on metasandstones in undeformed sections. They are represented mainly by dolomites intercalated with rare thin beds of shales, metagravelites, and metasandstones (Boreholes 3567, 3763, 3764, and 3838). The intercalated shale beds range in thickness from several millimeters to several meters and are composed of quartz and sericite, sometimes with an admixture of biotite and chlorite. In places, dolomites are silicified and, as a result of metamorphism, are altered to form calc-silicate rocks containing such minerals as calcite, quartz, feldspars, biotite, amphibole, and pyroxene.

ANALYTICAL PROCEDURES

The mineral composition of rocks was determined using a Jeol-6380 LV electron microscope equipped with an INCA Energy-250 energy-dispersive detector at the Voronezh State University. The conditions of the analysis were as follows: accelerating voltage, 20 kV; probe current, 10–15 nA; time of spectrum collection, 70 s; electron beam diameter in the near-surface layer of a specimen, usually 3–5 μm. ZAF correction when calculating oxides contents and estimate of accuracy were made using standard mathematical programs.

Rock-forming elements were determined using a S8 Tiger X-ray fluorescence spectrometer (Bruker AXS GmbH, Germany) at the Voronezh State University. Preparation of specimens for analysis was performed by melting of 0.5 g of powdered sample and 2 g of lithium tetraborate in a muffle furnace with subsequent casting of a glass-like disk. When calibrating the spectrometer and for quality control of measurements, we used state standards of chemical composition of rocks (GSO 8871-2007, GSO 3333-85, and GSO 3191-85). Analytical accuracy was 1–5% for elements with concentrations above 1–5% and up to 12% for elements with concentrations below 0.5%.

Minor and trace elements were determined by inductively coupled plasma mass spectrometry (ICP-MS) at the Analytical Certification Test Center (Institute of Microelectronics and High Purity Materials, Russian Academy of Sciences, Chernogolovka, Moscow oblast). Decomposition of rock specimens was implemented by acidolysis at 220°C. The detection limits for REEs, Hf, Ta, Th, and U were 0.02–0.03 μg/g; for Nb, Be, and Co, 0.03–0.05 μg/g; for Li, Ni, Ga, and Y, 0.1 μg/g; for Zr, 0.2 μg/g; for Rb, Sr, and Ba, 0.3 μg/g; for Cu, Zn, V, and Cr, 1–2 μg/g. Correctness of analysis was controlled by measuring standard specimens GSP-2, VM, SGD-1A, and ST-1. Errors in determination of concentrations for the majority of elements were from 3 to 5%.

The measurement of the isotopic composition of C and O in dolomites was performed using continuous flow isotope ratio mass spectrometry (CF-IRMS) in a helium flow by a modified technique (McCrea, 1950) on a DELTA V Advantage mass spectrometer equipped with a GasBench II system of preparation and introduction of specimens, at the Geonauka Center for Collective Use (Institute of Geology of the Komi Sci-

Table 1. Compositions (wt %) of carbonates from dolomites and calc-silicate rocks of the Ignateevo Formation

Sample no.	3759/504.5		3759/510	3759/511		3764/240.4				3764/241.5		
Components	Dol-1	Cal-2	Cal-2	Dol-1	Cal-3	Cal-2	Dol-3	Dol-7	Cal-9	Cal-2	Cal-6	Dol-7
SiO_2	–	–	0.36	–	–	–	–	–	–	–	0.33	–
FeO	2.26	–	0.41	2.91	–	0.52	2.78	2.40	–	–	–	3.49
MnO	0.61	0.36	–	0.73	0.72	0.54	0.53	0.27	0.72	0.71	0.76	0.48
MgO	17.93	–	0.90	18.94	1.03	0.95	18.16	22.38	0.88	1.87	0.59	17.72
CaO	27.95	50.74	50.36	28.74	49.58	49.54	28.01	24.95	48.39	46.52	45.68	27.66
Sum	48.75	51.10	52.03	51.32	51.33	51.55	49.48	50.00	49.99	49.10	47.36	49.35
Sample no.	3785/371.2					3785/390		3785/390				
Components	Cal-1	Cal-4	Cal-9	Cal-13	Cal-19	Cal-2	Cal-6	Dol-8	Cal-9	Cal-11	Cal-12	Dol-16
SiO_2	–	–	–	–	0.67	–	0.32	0.32	–	–	0.34	–
FeO	–	–	–	–	–	0.60	0.54	2.87	0.63	0.46	–	2.86
MnO	0.70	–	–	0.38	–	1.12	0.96	1.28	1.31	1.53	1.09	1.38
MgO	–	–	–	0.43	0.46	1.07	0.88	17.75	2.57	2.74	0.95	18.36
CaO	52.18	51.87	51.80	51.76	53.01	49.23	49.51	29.27	47.16	47.55	50.72	30.24
Sum	52.88	51.87	51.80	52.57	54.14	52.02	52.21	51.49	51.67	52.28	53.10	52.84

A dash means that the content of the element was below the detection limit. Here and in Tables 2–7, the number of sample represents the borehole no./depth.

entific Center, Ural Branch of the Russian Academy of Sciences, Syktyvkar). Dolomite powder was decomposed in orthophosphoric acid for 72 h at 60°C. The values of $\delta^{13}C$ and $\delta^{18}O$ are given in pro mille relative to the V-PDB standard (Table 7). In the calibration, we used the NBS-18, NBS-19, and Kh-2 international standards. The error in determinations of $\delta^{13}C$ and $\delta^{18}O$ was $\pm 0.2‰$ (1σ).

Rb–Sr systemization of specimens was examined by using selective dissolution (leaching) in 0.01 N solution of hydrochloric acid (Kuznetsov et al., 2005). Powdered specimens were first treated with this solution at room temperature. The extract and residue were separated by centrifuging, and then the residue enriched in primary carbonate material was treated with 0.5 N hydrochloric acid for a day at 60°C. The obtained solution was used for further study. The concentrations of Rb and Sr were determined by isotope dissolution using a mixed ^{87}Rb–^{84}Sr indicator, and for isotope analysis, we used a Finnigan MAT-261 multicollector mass spectrometer. The isotopic composition of Sr was measured on a Triton TI multicollector mass spectrometer. The measured $^{87}Sr/^{86}Sr$ ratio in strontium carbonate SRM 987 (NIST, United States) yielded 0.71029 ± 0.00001 ($n = 16$). The rubidium concentration in specimens did not exceed 0.03 μg/g and was not further taken into account. The error in measurements of the $^{87}Sr/^{86}Sr$ ratio in specimens was less than 0.008% (1σ). The level of laboratory contamination for Rb and Sr determined by blank experiments did not exceed 2.0 and 1.9 ng, respectively.

PETROGRAPHY AND MINERALOGY

Carbonate deposits of the Ignateevo Formation are represented by dolomite marbles and calc-silicate rocks. The rocks are metamorphosed and do not contain relics of layered sedimentary structures.

Dolomite Marbles

Dolomites are fine- and middle-grained, with banded, indistinctly banded, and massive structures and granoblastic texture. Dolomite crystals are hypidiomorphic, with polygonal outlines, up to 0.4–0.7 mm in size, less often more than 1.0 mm. Dolomite contains admixtures of iron (up to 3 wt % of FeO) and manganese (up to 1.5 wt % of MnO). On the basis of the results of microprobe analysis, dolomite marbles contain up to 15% of calcite, which in turn contains admixtures of magnesium (up to 1 wt % of MgO), iron (up to 3 wt % of FeO), and manganese (up to 2.3 wt % of MnO) (Table 1).

Dolomite marbles also contain an insignificant admixture (up to 5%) of such silicate minerals as tremolite, talc, biotite, and quartz. Tremolite is represented by prismatic colorless crystals (Samples 3759/504.5 and 3759/511) up to 5 mm in size and has a high magnesium content ($X_{Mg} = 0.89–0.94$) (Fig. 3, Table 2). Biotite is present in the form of fine (0.1–0.4 mm)

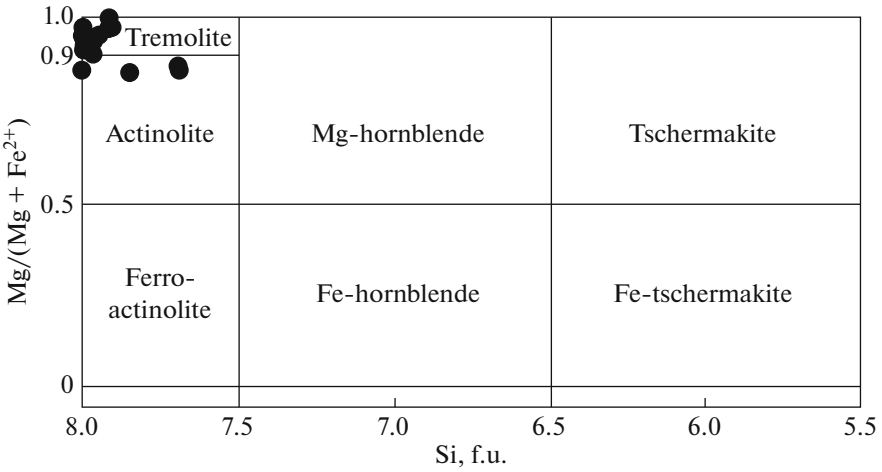

Fig. 3. Classification chart for amphiboles from the Ignateevo Formation dolomites.

light brown laths; it is distinguished by a low titanium content (<1 wt % of TiO_2) and a high magnesium content (X_{Mg} = 0.83–0.88) (Table 3). Talc and chlorite are secondary minerals replacing tremolite and biotite.

Calc-Silicate Rocks

In contrast to dolomites, calcite is the predominant mineral in calc-silicate rocks; in addition, significant amounts of feldspars, diopsides, tremolites, biotites, muscovites, and quartz are reported.

Calcite is represented by hypidiomorphic polygonal and tabular crystals with polysynthetic twins, up to 1 mm in size. The amounts of calcite in thin sections vary considerably, from 50% to less than 10%. In terms of composition, this is almost pure calcite with insignificant admixtures of iron (0.4–0.6 wt % FeO), magnesium (<3 wt % MgO), and manganese (<1 wt % MnO) (Table 1).

Dolomite is rarely found, mainly in rocks with the lowest amounts of quartz and silicate minerals (e.g., Sample 3764/240.4). Dolomite is represented not only by pure mineral crystals in calcite matrix but also by irregularly shaped inclusions in calcite. Dolomite always contains insignificant amounts of iron (2–3 wt % FeO) and manganese (up to 1.5 wt % MnO) (Table 1).

Diopside is found in the form of colorless tabular crystals with well-marked cleavage, less often in the form of rounded isometric grains usually showing no cleavage, ranging from 0.1 to 1 mm in size. Diopside crystals often intergrow, occupying considerable parts of thin sections. In terms of composition, diopside is close to the finite magnesian member of the isomorphic series, characterized by magnesium content of 88 to 100% (Table 4).

Amphibole is found in the form of elongated prismatic grains (0.3–1.2 mm) intergrown with carbonates and diopside; its amounts in calc-silicate rocks are larger than in dolomites. In terms of composition, amphiboles are low-alumina, excluding Sample 3764/233, where Al_2O_3 content is 3.4 wt % (Table 2). On the basis of the classification by Leak et al. (1997), amphiboles correspond to tremolite composition: (Ca + Na)B ≥ 1.34, NaB < 0.67, (Na + K)A < 0.50, Si > 7.50, 0.5 < Mg/(Mg + Fe) ≤ 1.0 (Fig. 3).

Biotite in calc-silicate rocks is reddish brown and sharply different in composition from biotite from dolomites owing to higher contents of iron (X_{Mg} = 0.54–0.81) and titanium (TiO_2 = 1.6–3.1 wt %) (Table 3).

Feldspars are represented by plagioclase and microcline. Plagioclase is present in the form of small prismatic grains, sometimes with polysynthetic twins 0.2–0.5 mm in cross size. The composition of plagioclases ranges considerably from almost pure albite (X_{An} = 0.03) to andesine (X_{An} = 0.42; Table 5). K-feldspar is represented by skeletal microcline with a very insignificant albite admixture.

Thus, main mineralogical difference between calc-silicate rocks and dolomite marbles are in appearance of feldspars and diopside and in a considerably larger amount of tremolite. Calcite is abruptly predominant over dolomite. Biotite is more ferruginous and tintaniferous. These differences are determined by the influence of metamorphism on mineral parageneses as a result of reactions of quartz-containing dolomite decarbonization leading to formation of tremolite and calcite ($8Qtz + 5Dol + H_2O \rightarrow 3Cal + Tr + 7CO_2$) and, eventually, diopside ($Tr + 2Qtz + 3Cal \rightarrow Di + 3CO_2 + H_2O$).

GEOCHEMISTRY

Dolomite Marbles

Dolomite marbles have a more consistent composition relative to calc-silicate rocks and do not show clearly marked silicification (no more than 4 wt % of

Table 2. Compositions of amphiboles from carbonate rocks of the Ignateevo Formation

Sample no.	3759/504.5	3759/507.5	3759/510	3759/511	3764/233		3764/240.4	3764/241.5	
Components	Am-3	Am-3	Am-1	Am-2	Am-1	Am-6	Am-8	Am-1	Am-5
SiO_2	58.99	58.63	58.23	57.80	55.09	54.88	58.51	57.95	58.30
TiO_2	–	–	–	–	–	–	–	–	–
Al_2O_3	–	0.63	–	0.49	2.81	3.40	0.60	0.48	0.48
Cr_2O_3	–	–	–	–	–	–	–	–	–
FeO	2.86	2.89	4.00	3.33	8.56	7.58	3.15	2.50	2.84
MnO	–	–	0.54	–	–	0.54	–	0.39	–
MgO	22.91	22.87	22.49	22.20	18.75	18.41	22.54	22.98	23.15
CaO	13.50	13.49	13.03	13.99	13.11	12.78	13.54	13.44	12.96
Na_2O	–	–	–	–	–	–	–	–	–
K_2O	–	–	–	–	–	0.22	–	–	–
Sum	**98.25**	**98.51**	**98.28**	**97.80**	**98.33**	**97.82**	**98.33**	**97.74**	**97.73**
Si	8.03	7.95	7.92	7.98	7.66	7.66	7.97	7.92	7.92
Al^{IV}	–	0.05	–	0.02	0.34	0.34	0.03	0.08	0.08
Ti	–	–	–	–	–	–	–	–	–
Σ	**8.03**	**8.00**	**7.92**	**8.00**	**8.00**	**8.00**	**8.00**	**8.00**	**8.00**
Al	–	0.05	–	0.06	0.12	0.22	0.07	–	–
Ti	–	–	–	–	–	–	–	–	–
Cr^{3+}	–	–	–	–	–	–	–	–	–
Fe^{3+}	–	0.08	0.35	–	0.31	0.29	0.01	0.16	0.32
Mn^{3+}	–	–	0.06	–	–	0.06	–	0.05	–
Mg	4.64	4.62	4.56	4.56	3.88	3.83	4.57	4.68	4.68
Fe^{2+}	0.32	0.25	0.03	0.38	0.68	0.59	0.35	0.11	–
Σ	**4.96**	**5.00**	**5.00**	**5.00**	**4.99**	**4.99**	**5.00**	**5.00**	**5.00**
Mg	–	–	–	–	–	–	–	–	–
Fe^{2+}	–	–	0.07	0.17	–	–	–	0.02	–
Ca	1.97	1.96	1.90	2.07	1.95	1.91	1.98	1.97	1.88
Na	–	–	–	–	–	–	–	–	–
Σ	**1.97**	**1.96**	**1.97**	**2.24**	**1.95**	**1.91**	**1.98**	**1.99**	**1.88**
Na	–	–	–	–	–	–	–	–	–
K	–	–	–	–	–	–	–	–	–
X_{Mg}	0.94	0.95	0.98	0.89	0.85	0.86	0.93	0.97	1.00

Table 2. (Contd.)

Sample no.	3785/371.2						3785/390		3785/391
Components	Am-5	Am-10	Am-11	Am-12	Am-15	Am-18	Am-3	Am-5	Am-3
SiO_2	58.33	58.34	58.12	59.10	58.71	59.04	56.52	55.64	56.19
TiO_2	–	–	–	–	–	–	–	–	–
Al_2O_3	–	–	–	–	–	–	2.21	3.10	2.00
Cr_2O_3	–	–	–	–	–	–	–	–	–
FeO	3.76	4.08	4.04	2.96	3.46	3.03	3.25	5.61	5.99
MnO	0.38	0.34	0.64	0.36	0.39	–	0.91	0.52	–
MgO	22.29	21.36	21.89	22.87	22.22	22.94	22.13	20.33	20.03
CaO	13.83	13.47	13.16	13.27	13.53	12.80	12.65	12.95	13.84
Na_2O	–	0.53	–	–	–	–	0.37	–	–
K_2O	–	–	–	–	–	–	–	0.29	–
Sum	**98.59**	**98.13**	**97.85**	**98.56**	**98.32**	**97.80**	**98.04**	**98.45**	**98.06**
Si	7.98	8.08	7.98	8.01	8.03	8.02	7.69	7.64	7.82
Al^{IV}	–	–	–	–	–	–	0.31	0.36	0.18
Ti	–	–	–	–	–	–	–	–	–
Σ	**7.98**	**8.08**	**7.98**	**8.01**	**8.03**	**8.02**	**8.00**	**8.00**	**8.00**
Al	–	–	–	–	–	–	0.04	0.14	0.15
Ti	–	–	–	–	–	–	–	–	–
Cr^{3+}	–	–	–	–	–	–	–	–	–
Fe^{3+}	–	–	0.16	0.13	–	0.24	–	0.37	–
Mn^{3+}	0.04	0.04	0.07	0.04	0.04	–	0.10	0.06	–
Mg	4.54	4.41	4.48	4.62	4.53	4.64	4.48	4.16	4.15
Fe^{2+}	0.42	0.55	0.29	0.20	0.42	0.10	0.37	0.27	0.70
Σ	**5.00**	**5.00**	**5.00**	**4.99**	**4.99**	**4.98**	**4.99**	**5.00**	**5.00**
Mg	–	–	–	–	–	–	–	–	–
Fe^{2+}	0.03	0.22	0.01	–	–	–	–	0.01	0.10
Ca	2.03	2.00	1.94	1.92	1.98	1.86	1.84	1.90	2.06
Na	–		–	–	–	–	0.10	–	–
Σ	**2.06**	**2.22**	**1.95**	**1.92**	**1.98**	**1.86**	**1.94**	**1.90**	**2.16**
Na	–	0.14	–	–	–	–	–	–	–
K	–	–	–	–	–	–	–	0.05	–
OH	2.00	2.00	2.00	2.00	2.00	2.00	2.00	2.00	2.00
X_{Mg}	0.91	0.85	0.94	0.96	0.91	0.98	0.92	0.94	0.84

Table 3. Compositions of biotites from carbonate rocks of the Ignateevo Formation

Sample no.	3764/240.4		3785/323.8				3785/390					3785/391		3785/460
Components	Bt-1	Bt-4	Bt-3	Bt-4	Bt-10	Bt-12	Bt-1	Bt-10	Bt-13	Bt-14	Bt-15	Bt-4	Bt-7	Bt-2
SiO_2	39.93	38.62	37.49	37.69	37.68	37.36	39.67	39.62	41.20	40.23	39.88	40.47	39.31	36.38
TiO_2	0.52	0.98	2.33	1.94	1.59	1.59	0.87	0.40	0.53	0.40	0.34	1.88	1.66	3.11
Al_2O_3	14.52	17.33	16.05	16.29	16.88	16.02	17.19	16.77	14.75	15.78	15.84	16.84	15.92	18.14
FeO	6.47	5.78	17.15	16.84	16.74	18.24	7.19	6.16	5.45	5.52	6.22	8.11	9.16	16.38
MnO	–	–	–	–	–	0.44	–	–	–	–	0.51	–	–	–
MgO	22.67	22.30	12.17	13.01	12.95	12.47	20.24	22.10	23.35	23.16	22.33	19.11	19.11	10.68
CaO	0.39	–	–	–	–	–	–	–	0.27	–	–	–	–	–
Na_2O	–	–	–	–	–	–	–	0.48	0.51	0.37	–	–	–	0.45
K_2O	10.55	10.49	9.80	9.24	9.92	9.46	9.75	9.89	9.68	9.89	10.32	9.43	9.77	9.58
Sum	**95.04**	**95.51**	**94.99**	**95.02**	**95.76**	**95.58**	**94.91**	**95.42**	**95.74**	**95.34**	**95.44**	**95.84**	**94.92**	**94.72**
Si	2.89	2.78	2.91	2.91	2.88	2.88	2.91	2.85	2.94	2.89	2.88	2.97	2.91	2.83
Al	1.11	1.22	1.09	1.09	1.12	1.12	1.09	1.15	1.06	1.11	1.12	1.03	1.09	1.17
Σ	**4.00**	**4.00**	**4.00**	**4.00**	**4.00**	**4.00**	**4.00**	**4.00**	**4.00**	**4.00**	**4.00**	**4.00**	**4.00**	**4.00**
Al	0.13	0.25	0.38	0.39	0.40	0.34	0.39	0.27	0.19	0.22	0.23	0.43	0.31	0.50
Fe	0.39	0.35	1.11	1.09	1.07	1.18	0.44	0.37	0.32	0.33	0.37	0.50	0.57	1.06
Mg	2.45	2.39	1.41	1.50	1.47	1.43	2.21	2.37	2.49	2.47	2.40	2.09	2.11	1.24
Ti	0.03	0.05	0.14	0.11	0.09	0.09	0.05	0.02	0.03	0.02	0.02	0.10	0.09	0.18
Mn	–	–	–	–	–	0.03	–	–	–	–	0.03	–	–	–
Ca	0.03	–	–	–	–	–	–	–	0.02	–	–	–	–	–
Na	–	–	–	–	–	–	–	0.07	0.07	0.05	–	–	–	0.07
Σ	**3.03**	**3.04**	**3.04**	**3.09**	**3.03**	**3.07**	**3.09**	**3.10**	**3.12**	**3.09**	**3.05**	**3.12**	**3.08**	**3.05**
K	0.97	0.96	0.97	0.91	0.97	0.93	0.91	0.91	0.88	0.90	0.95	0.88	0.92	0.95
X_{Mg}	0.86	0.87	0.56	0.58	0.58	0.54	0.83	0.86	0.88	0.88	0.86	0.81	0.79	0.54

Table 4. Compositions of diopsides from calc-silicate rocks of the Ignateevo Formation

Sample no.	3759/507.5					3785/371.2			3785/391	
Components	Di-1	Di-2	Di-4	Di-5	Di-6	Di-7	Di-14	Di-17	Di-2	Di-8
SiO_2	55.32	55.15	54.98	53.96	55.46	48.37	55.62	54.56	54.88	55.09
TiO_2	–	–	–	–	–	–	–	–	–	–
Al_2O_3	–	–	–	–	–	–	–	–	–	0.41
Cr_2O_3	–	–	–	–	–	–	–	–	–	–
FeO	2.07	3.75	0.70	2.55	0.75	3.53	1.84	1.37	3.63	3.77
MnO	0.53	0.77	–	–	–	0.66	0.40	0.37	0.54	–
MgO	18.63	15.44	18.62	17.02	18.09	17.90	17.21	17.89	16.40	15.97
CaO	25.27	25.74	25.67	26.09	25.12	28.89	25.38	25.39	25.36	24.54
Na_2O	–	–	–	–	–	–	–	–	–	–
K_2O	–	–	–	–	–	–	–	–	–	–
Sum	101.82	100.84	99.98	99.62	99.42	99.35	100.45	99.58	100.81	99.78
Si	1.97	2.01	1.98	1.97	2.02	1.77	2.02	1.99	2.00	2.03
Ti	–	–	–	–	–	–	–	–	–	–
Al	–	–	–	–	–	–	–	–	–	0.02
Cr	–	–	–	–	–	–	–	–	–	–
Fe^{3+}	0.06	–	0.03	0.05	–	0.47	–	0.03	0.01	–
Fe^{2+}	–	0.11	–	0.02	0.02	–	0.06	0.01	0.10	0.12
Mn	0.02	0.02	–	–	–	0.02	0.01	0.01	0.02	–
Mg	0.99	0.84	1.00	0.93	0.98	0.97	0.93	0.97	0.89	0.87
Ca	0.96	1.01	0.99	1.02	0.98	1.13	0.99	0.99	0.99	0.97
Na	–	–	–	–	–	–	–	–	–	–
K	–	–	–	–	–	–	–	–	–	–
X_{Mg}	0.98	0.86	1.00	0.97	0.98	0.98	0.93	0.97	0.88	0.88

Table 5. Compositions of feldspars from calc-silicate rocks of the Ignateevo Formation

Sample no.	3764/233					3785/323.8				3785/391	3785/460
Components	Kfs-2	Pl-3	Kfs-5	Pl-7	Pl-8	Pl-1	Pl-2	Kfs-7	Pl-11	Pl-1	Kfs-1
SiO_2	64.19	56.79	65.06	64.18	61.23	61.11	59.77	64.70	62.46	58.31	63.65
Al_2O_3	18.30	26.91	18.57	22.26	24.63	23.75	24.70	18.94	23.90	26.71	18.61
FeO	–	–	–	–	–	–	–	–	–	–	–
CaO	–	8.77	–	0.60	4.30	5.01	6.64	–	5.19	7.45	–
Na_2O	0.55	6.39	0.56	10.46	8.29	9.32	7.48	0.78	8.97	7.07	0.76
K_2O	15.85	0.62	15.82	1.72	1.72	–	0.26	15.35	0.17	0.61	15.15
Sum	**98.89**	**99.48**	**100.02**	**99.22**	**100.17**	**99.19**	**98.85**	**100.54**	**100.70**	**100.15**	**98.17**
Si	3.00	2.56	3.01	2.83	2.71	2.72	2.70	2.99	2.74	2.60	2.99
Al^{IV}	1.01	1.43	1.01	1.16	1.28	1.24	1.31	1.03	1.24	1.40	1.03
Fe^{3+}	–	–	–	–	–	–	–	–	–	–	–
Σ	**4.01**	**3.99**	**4.02**	**3.99**	**3.99**	**3.96**	**4.01**	**4.02**	**3.98**	**4.00**	**4.02**
Ca	–	0.42	–	0.03	0.20	0.24	0.32	–	0.24	0.36	–
Na	0.05	0.56	0.05	0.89	0.71	0.80	0.65	0.07	0.76	0.61	0.07
K	0.94	0.04	0.93	0.10	0.10	–	0.01	0.91	0.01	0.03	0.91
Σ	**0.99**	**1.02**	**0.98**	**1.02**	**1.01**	**1.04**	**0.98**	**0.98**	**1.01**	**1.00**	**0.98**
Ort	0.95	0.04	0.95	0.09	0.10	–	0.02	0.93	0.01	0.03	0.93
Ab	0.05	0.55	0.05	0.88	0.70	0.77	0.66	0.07	0.75	0.61	0.07
An	–	0.42	–	0.03	0.20	0.23	0.32	–	0.24	0.36	–

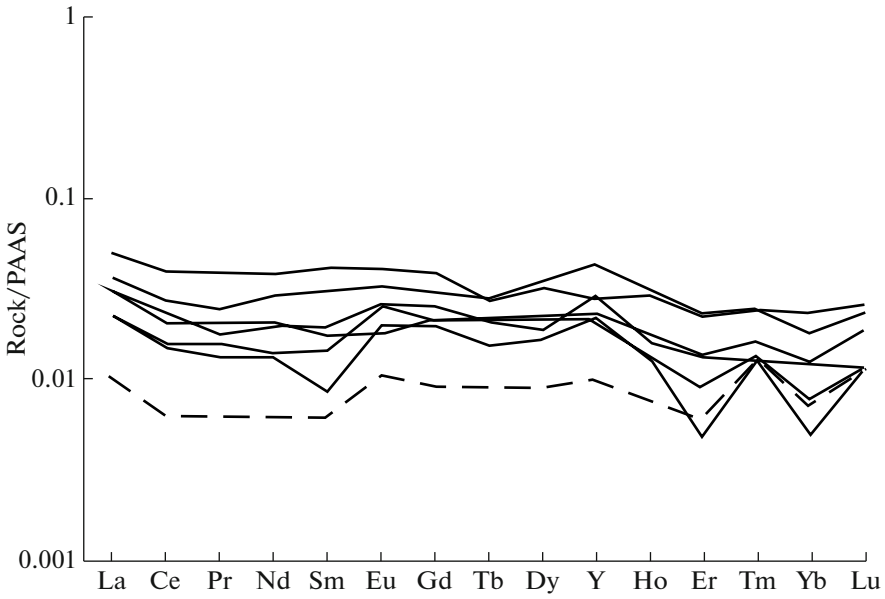

Fig. 4. REE + Y distribution in the Ignateevo Formation dolomites normalized to the Post-Archean Australian Shale (PAAS; Condie, 1993). Pseudolanthanide yttrium (Y) is inserted between Ho and Dy in accordance with its identical charge and analogous radius (REE + Y model; Bau and Dulski, 1996).

SiO_2; 2 wt % on average). The contents of Al_2O_3 do not exceed 1 wt % (Table 6) and show no correlation with SiO_2. In addition, we established quite constant concentrations of CaO (29–31 wt %), MgO (21–22 wt %, excluding one specimen with 17.8 wt %), and FeO (2–3 wt %, excluding one specimen). Dolomite marbles are characterized by low concentrations of the other petrogenic oxides, such as Na_2O, K_2O, TiO_2, and P_2O_5 (Table 6).

Dolomites have very low concentrations of such rare elements (Table 6) as Rb (<2 μg/g), Cs (<0.2 μg/g), Sc (<0.6 μg/g), Zr (<7 μg/g), Nb (<0.5 μg/g), and Th (<0.5 μg/g). Additionally, low concentrations of Sr (23–67 μg/g; mean value is 32 μg/g) and Ba (<7.4 μg/g) are reported.

Dolomites are characterized by relatively low concentrations of rare-earth elements (ΣREE = 3.3–7.9 μg/g; mean value is 4.5 μg/g), ΣLREE = 0.8–5.0 μg/g, ΣHREE = 0.1–0.5 μg/g, and flat distribution with an insignificant enrichment in LREE (Pr_{SN}/Yb_{SN} = 1.2–2.7; mean value is 1.7) (Fig. 4). They contain no marked Ce anomalies (Ce/Ce* = 0.8–0.9) and demonstrate positive anomalies of Eu (Eu/Eu* = 0.95–1.65; mean value is 1.3) and La (La/La* = 1.1–2.1; mean value is 1.6). The Y/Ho ratio in dolomites (38 on average) is higher than the chondrite one (32) and PAAS (27) (Condie, 1993).

The values of $\delta^{13}C$ in the Ignateevo Formation dolomites vary from +0.3 to +0.9‰ PDB, while those of $\delta^{18}O$ vary from –13 to –9.2‰ PDB (Table 7). The $^{87}Sr/^{86}Sr$ ratio in the Ignateevo Formation dolomites is within the range of 0.71014–0.71951 (Table 7).

Calc-Silicate Rocks

Calc-silicate rocks are distinct in different degrees of silicification and, hence, broad variations in compositions: 13–63 wt % SiO_2, up to 6 wt % Al_2O_3, 11–18 wt % MgO, and 16–33 wt % CaO (Table 6). They demonstrate low contents of the other petrogenic oxides, such as K_2O, Na_2O, TiO_2, MnO, and Fe_2O_{3tot}. There is no correlation between the SiO_2 and Al_2O_3 concentrations. Obviously, calc-silicate rocks having higher Al_2O_3 contents (>3 wt %) are enriched in detrital material.

Calc-silicate rocks having low Al_2O_3 contents (without enrichment in detrital material) show even lower concentrations of lithophile elements in comparison with dolomites (Table 6): Rb (<2 μg/g), Cs (<0.1 μg/g), Sc (0.3 μg/g), Zr (8 μg/g), Nb (<0.5 μg/g), and Th (<0.1 μg/g). In addition, they have very low contents of Sr (13 μg/g) and Ba (<3 μg/g) (Table 6).

Calc-silicate rocks are characterized by low REE concentrations (ΣREE = 1.8 μg/g, ΣLREE = 0.8 μg/g, ΣHREE = 0.12 μg/g) and flat REE distribution with an insignificant enrichment in HREE (Pr_{SN}/Yb_{SN} = 0.9) (Fig. 4). They show no Ce anomaly (Ce/Ce* = 0.8), but exhibit a positive Eu anomaly (Eu/Eu* = 1.4). The Y/Ho ratio (32.7 on average) is close to the chondrite one.

The values of $\delta^{13}C$ and $\delta^{18}O$ in calc-silicate rocks are very low, reaching –5.3 and –15.6‰ PDB, respectively (Table 7).

Table 6. Contents of petrogenic (wt %), rare and rare earth elements (μg/g) in carbonate rocks of the Ignateevo Formation

Rocks	Dolomites								Calc-silicate rocks					
Sample no.	3785/ 387	3785/ 364	3759/ 504.5	3759/ 511	3759/ 513	3767/ 403.4	3785/ 386	3759/ 493	3759/ 505.6	3759/ 510	3759/ 507.5	3764/ 241.5	3764/ 240.4	3567/ 375.7
SiO_2	0.86	2.55	2.84	3.95	1.15	2.72	2.10	–	39.54	63.24	57.54	24.02	12.68	16.38
TiO_2	0.01	0.02	–	–	0.01	0.02	0.06	0.01	–	–	–	0.49	0.17	0.11
Al_2O_3	0.33	0.57	0.09	0.10	0.44	1.03	0.23	0.25	0.11	0.07	0.07	5.65	3.30	4.42
Fe_2O_{3tot}	2.27	2.09	2.25	2.64	2.12	0.48	2.23	2.59	2.14	1.66	2.91	4.66	3.27	1.42
MgO	21.02	21.54	21.56	20.91	21.67	22.28	21.98	17.82	15.44	11.33	13.91	15.33	14.55	18.32
MnO	0.411	0.395	0.471	0.463	0.518	0.337	0.46	0.531	0.444	0.28	0.467	0.34	0.389	0.293
CaO	29.54	29.68	31.04	30.79	30.35	29.05	29.04	31.06	28.14	16.51	23.18	27.66	32.70	23.59
Na_2O	–	–	–	–	–	0.05	–	0.06	–	–	–	0.05	–	–
K_2O	0.02	0.05	0.01	–	–	0.33	0.05	0.03	–	0.01	–	3.44	1.65	2.05
P_2O_5			–	–	–	0.01	–	–	–		–	0.12	0.05	0.02
L.O.I.	44.82	43.02	41.7	41.09	43.59	43.65	43.85	47.64	14.15	6.83	1.85	18.06	31.01	33.32
Sum	99.90	99.90	99.90	99.90	99.90	99.90	99.90	99.90	99.90	99.90	99.90	99.90	99.90	99.90
MgO/CaO	0.71	0.73	0.69	0.68	0.71	0.77	0.76	0.57	0.55	0.69	0.60	0.55	0.44	0.78
Be		<1	<1	<1	<1	<1	<1	0.05		<1				
Sc		0.34	<0.2	<0.2	0.37	0.43	<0.2	0.59		0.33				
V		3	<2.5	<2.5	2.55	4.51	<2.5	3.51		8.97				
Cr		5.24	1.16	1.03	3.81	5.81	2.44	18.63		10				
Co		1.49	<0.5	0.53	0.7	0.89	0.67	1.60		<0.5				
Ni		6.91	2.01	2.65	5.83	3.36	7.68	16.18		6.28				
Cu		54.2	23.1	23.8	20.7	27.3	29.5	2.84		23				
Zn		33.1	18.2	22	19.4	58	24.9	86.50		19.1				
Ga		0.72	0.17	0.25	0.51	1.08	0.35	0.51		0.29				
Rb		<2	<2	<2	<2	7.6	<2	1.49		<2				
Sr		25.6	32.8	33	22.9	24.1	66.9	54.64		12.7				
Y		1.18	0.58	0.59	0.63	0.74	0.78	0.74		0.27				
Zr		3.05	1.38	0.99	3.28	7.16	1.31	2.50		8.43				
Nb		<0.5	<0.5	<0.5	<0.5	<0.5	<0.5	0.20		<0.5				
Mo		<0.6	<0.6	<0.6	0.7	<0.6	<0.6	0.13		<0.6				
Sn		0.71	0.69	0.83	0.6	0.72	0.59	0.21		1.09				
Cs		0.3	<0.1	<0.1	<0.1	0.21	<0.1	0.08		<0.1				
Ba		7.38	<3	<3	<3	18.1	6.42	5.38		<3				
La		1.39	0.86	0.87	1.16	1.89	1.13	1.08		0.38				

Table 6. (Contd.)

Rocks	Dolomites								Calc-silicate rocks					
Sample no.	3785/ 387	3785/ 364	3759/ 504.5	3759/ 511	3759/ 513	3767/ 403.4	3785/ 386	3759/ 493	3759/ 505.6	3759/ 510	3759/ 507.5	3764/ 241.5	3764/ 240.4	3567/ 375.7
Ce		2.21	1.27	1.22	1.65	3.18	1.74	1.79		0.51				
Pr		0.22	0.14	0.12	0.18	0.35	0.16	0.20		0.058				
Nd		0.93	0.44	0.42	0.66	1.23	0.63	0.76		0.21				
Sm		0.17	0.081	0.048	0.098	0.23	0.11	0.10		0.036				
Eu		0.036	0.028	0.022	0.02	0.045	0.029	0.03		0.012				
Eu		0.035	0.03	0.024	0.023	0.05	0.024			0.012				
Gd		0.14	0.1	0.093	0.1	0.18	0.12	0.12		0.043				
Tb		0.022	0.016	0.012	0.016	0.021	0.016	0.01		0.007				
Dy		0.15	0.09	0.073	0.097	0.14	0.082	0.17		0.04				
Ho		0.03	0.013	0.013	0.017	0.029	0.016	0.02		0.0083				
Er		0.067	0.026	0.014	0.039	0.064	0.038	0.06		0.017				
Tm		0.0096	0.0054	0.005	0.0064	0.0097	0.005	0.01		0.005				
Yb		0.05	0.022	0.014	0.035	0.065	0.034	0.05		0.02				
Lu		0.01	0.005	0.005	0.008	0.011	0.005			0.005				
Hf		0.099	0.045	<0.01	0.072	0.2	0.051	0.06		0.15				
Ta		<0.1	<0.1	<0.1	<0.1	<0.1	<0.1	0.02		<0.1				
W		<0.5	<0.5	<0.5	<0.5	<0.5	<0.5	0.11		<0.5				
Pb		<1.0	<1.0	1.24	<1.0	1.4	2.27	1.50		<1.0				
Th		0.33	<0.1	<0.1	0.3	0.54	0.17	0.08		<0.1				
U		0.12	<0.1	<0.1	0.19	<0.1	<0.1	0.05		<0.1				
∑REE		6.51	3.39	3.27	4.73	7.91	4.57	5.33		1.83				
LREE		3.566	1.959	1.83	2.608	5.035	2.669	2.88		0.826				
HREE		0.4486	0.2594	0.206	0.3014	0.4907	0.29	0.42		0.127				
Eu/Eu*		1.11	1.44	1.66	0.95	1.20	1.30	1.33		1.406				
Y/Ho		39.3	44.6	45.4	37.1	25.5	48.8	37.0		32.5				
Ce/Ce*		0.842	0.873	0.847	0.806	0.902	0.880	0.856		0.77				
$(Gd/Yb)_n$		1.67	2.71	3.96	1.70	1.65	2.10	1.41		1.28				
$(La/Yb)_n$		2.1	2.9	4.6	2.4	2.1	2.45	1.59		1.4				
Sr/Y		21.7	56.6	55.9	36.3	32.6	85.8	73.5		47.0				
La/Yb		27.8	39.1	62.1	33.1	29.1	33.2	21.5		19.0				
Prs_N/Ybs_N		1.38	2.00	2.70	1.62	1.69	1.48	1.24		0.91				

Table 7. Isotope-geochemical composition of dolomites and calc-silicate rocks of the Ignateevo Formation

Sample no.	Mn, μg/g	Fe, μg/g	Sr, μg/g	$\delta^{13}C_{dol}$, ‰ PDB	$\delta^{18}O_{dol}$, ‰ PDB	$^{87}Sr/^{86}Sr$
Dolomites, Ignateevo Formation, Kursk block						
3759/513	5200	21200	21	0.9	−10.1	0.71014
3785/386	4600	22300	56	0.5	−11.3	0.71244
3785/387	4110	22700	38	0.6	−11.3	–
3767/504.5	4700	22500	30	0.3	−11.4	0.71236
3759/511	4600	26400	30	0.3	−11.6	0.71306
3767/403.4	3400	4800	21	0.8	−13.0	0.71951
Calc-silicate rocks, Ignateevo Formation, Kursk block						
3759/510	2800	16600	15	−5.3	−15.6	–

SEDIMENTATION CONDITIONS OF THE IGNATEEVO FORMATION CARBONATE DEPOSITS

The geochemical characteristics of carbonate deposits are important criteria for reconstructing sedimentation conditions. The distributions of many elements in carbonate rocks are controlled by the distance to the continent and also by the depths and tectonic settings of sedimentation basins. When assessing the degree of post-diagenetic and metamorphic alteration of carbonate rocks and in order to use them for the purposes of isotope chemostratigraphy, geochemical criteria are applied, namely, the Mg/Ca, Fe/Sr, and Mn/Sr ratios (Veizer et al., 1990, 1992; Kuznetsov et al., 2003, 2018; Melezhik et al., 2006, 2014, 2015; Gorokhov et al., 2016). This is due to the fact that recrystallization of carbonate rocks usually leads to enrichment in Mn and Fe, but depletion in Sr. The Mn and Fe concentrations in dolomite marbles of the Ignateevo Formation are very high (3400–5200 and 4800–26 400 μg/g, respectively), while Sr has low concentration (21–56 μg/g). Precambrian dolomites having these parameters imply epigenetic recrystallization accompanied by disturbance of the initial Rb–Sr isotope system; therefore, the broad variations of the $^{87}Sr/^{86}Sr$ ratio in dolomite marbles of the Ignateevo Formation (0.71014–0.71951) do not reflect the true Sr-isotope characteristic of the paleoocean.

Rocks of the Ignateevo Formation were subjected to metamorphism ca. 2.07 Ga (Savko et al., 2018). This event largely changed the initial isotope-geochemical characteristic of rocks. However, some geochemical signatures give us a clue to understanding of sedimentation conditions for the carbonate deposits of the studied formation. For example, analysis of REE distribution, which remains unchanged after diagenesis and recrystallization of carbonates, is a useful tool (Banner, 1995; Zhong and Mucci, 1995; Kamber and Webb, 2001; Van Kranendonk et al., 2003; Bau and Alexander, 2006; Allwood et al., 2010; Tang et al., 2016; Franchi, 2018).

Dolomitization of primary carbonates of the Ignateevo Formation sediments occurred at the stage of early diagenesis, analogous to many Archean and Paleoproterozoic sedimentary limestones in the Kaapvaal (Beukes, 1987) and Pilbara cratons (Veizer et al., 1990) and in Fennoscandia (Kuznetsov et al., 2010). Despite the obvious difference in chemical composition of the ocean waters in the Archean and Paleoproterozoic (Knauth, 1979; Hesse, 1989), calcareous sediments with a high Sr content (over 500–1500 μg/g) were predominant in the Precambrian paleooceans (Veizer et al., 1990; Gorokhov et al., 1998; Frauenstein et al., 2009; Kuznetsov et al., 2018, 2019). Ancient dolomites could have precipitated in shallow lagoons from very saline waters, and the Sr content in them could have reached 250–550 μg/g (Tucker and Wright, 1990; Warren, 2000; Kuznetsov et al., 2010). The Ignateevo Formation dolomites are characterized by mean Sr contents of 32 μg/g, which could have been caused either by very low Sr content in seawater or by loss of Sr under diagenesis/metamorphism. We think that depletion in Sr occurred as a result of dolomitization of carbonate sediments during diagenesis, as was described in many publications (Beukes, 1987; Bau and Alexander, 2006; Frauenstein et al., 2009; Kuznetsov et al., 2010). These conditions are characteristic of internal regions of platforms where reduced inflow of sea waters led to the formation of Mg-enriched solutions and complete dolomitization of carbonate deposits of the Ignateevo Formation.

Silicification, which is typical of dolomite sediments of the Ignateevo Formation, is a usual feature of Early Precambrian carbonate deposits, because sea waters at the end of the Neoarchean were oversaturated with silica and undersaturated with carbonate ions (Knauth, 1979; Hesse, 1989). Silicification during early diagenesis was related to the interaction of sea and meteoric waters in coastal sediments, especially under the conditions of higher porosity, increased salinity, reduced pH, and growth of fCO_2 (Knauth, 1979; Maliva and Siever, 1989). Replace-

ment of carbonates with silica could also have been caused by microbiological activity, through its influence on solubility of carbonates at the reduction in pH and silica precipitation (Hesse, 1989). These conditions took place in the carbonate platform of the Kaapvaal craton during silicification of Malmani dolomites at 2.6–2.5 Ga (Eroglu et al., 2017). Similar favorable conditions probably developed in the Ignateevo dolomite paleobasin during formation of its calc-silicate rocks. These conditions existed until accumulation of terrigenous deposits of the Stoilo Formation and ferruginous quartzites of the Korobki Formation. (Figs. 1c, 2).

The REE distribution in the Ignateevo Formation dolomites exhibits a significant similarity to that in carbonate rocks typical of Archean oceans: absence of Ce anomaly, positive La anomaly, and higher, compared to chondrite, Y/Ho ratio (Bau and Dulski, 1996; Kamber and Webb, 2001; Allwood et al., 2010).

The Ce anomaly is used for assessing the relative behavior of Ce, taking into account adjacent LREE, and is determined by the relation Ce = Ce/Ce*, where the Ce* value is obtained by linear interpolation between La and Nd values normalized to PAAS (Zhang et al., 2017). Ce is the only rare earth element that can be oxidized in natural environments; hence, it is sensitive to changes in seawater redox potential (Kamber and Webb, 2001). The absence of Ce anomalies is considered as evidence for carbonate precipitation from oxygen-less waters of Archean oceans (Kamber and Webb, 2001; van Kranendonk et al., 2003).

The Eu anomaly is determined by the relation Eu = Eu/Eu*, where the Eu* value is obtained by linear interpolation between the Sm and Tb values normalized to PAAS (Zhang et al., 2017). A positive Eu anomaly observed in Archean marine sediments is a direct indication that oceans did not contain oxygen and were drained by bottom high-temperature hydrothermal solutions (in deep basins) that were REE sources (Derry and Jacobsen, 1990; Bau and Dulski, 1999; Kamber and Webb, 2001). On the other hand, dolomites of the Transvaal Supergroup show that positive Eu anomalies (1.28 on average) can be considered as signs of epigenetic alteration of carbonate rocks due to metasomatic effect of fluids (Franchi, 2018).

The Y/Ho ratio is used as an indicator of circulation of hydrothermal solutions in a sedimentation basin and as that of REE fractionation (Nozaki et al., 1997; Bau and Dulski, 1999; Franchi et al., 2015, 2017). The study of Paleoproterozoic marine sediments showed that intense hydrothermal supply is characterized by the chondrite Y/Ho ratio, whereas the Y/Ho ratio in surface waters and associated marine sediments is superchondrite, which is the same as in modern seawater (Bau and Dulski, 1999; Franchi et al., 2017, and references therein). Thus, given a higher Y/Ho ratio (38 on average) reported in the Ignateevo Formation dolomites, we think there was no intense hydrothermal inflow. The observed positive Eu anomaly reported in the Ignateevo Formation dolomites is related to metamorphic recrystallization under the conditions of epidote-amphibolite facies.

Very low concentrations of TiO_2, Al_2O_3, Na_2O, K_2O, Zr, Sc, and Th in the Ignateevo Formation dolomites indicate the absence of significant input of silicoclastic material to the sedimentation paleobasin. Interestingly, calc-silicate rocks (silicified dolomites) at SiO_2 concentrations of 57–63 wt % contain as little as 0.07 wt % of Al_2O_3 and negligible amounts of lithophile elements, which also suggests reduced input of silicoclastic material (Table 6).

Neoarchean sea waters were usually characterized by the $\delta^{18}O$ values of about −8‰ PDB (Veizer et al., 1990, 1992). The $\delta^{18}O$ values in the Ignateevo Formation dolomites (from −13.0 to −10.1‰ PDB) are slightly less than this (Table 7, Fig. 5), probably indicating the interaction with hydrothermal fluids during the early diagenesis under dolomitization and silicification. The observed decrease in $\delta^{18}O$ values by 2‰ in the Ignateevo Formation dolomites could have occurred during the interaction of diagenetic dolomites with meteoric and deep waters.

The values of $\delta^{13}C$ in the Ignateevo Formation dolomites vary within a narrow range from 0.3 to 0.9‰ PDB (Table 7, Fig. 5), falling within the domain of typical Neoarchean and Early Paleoproterozoic marine carbonates (Veizer et al., 1990, 1992; Bekker, 2001; Frauenstein et al., 2009; Kuznetsov et al., 2010).

Thus, at the end of the Archean, a sedimentary basin was initiated in Eastern Sarmatia on the craton that consolidated at 2.8 Ga (Savko et al., 2018), and accumulation of terrigenous and chemogenic sediments began there. Accumulation of coarse deposits of the Ignateevo Formation in the Mikhailovka synform and their abrupt change through gravelites and sandstones to carbonates indicate a rapid transgression that began in the western part of Eastern Sarmatia (Savko et al., 2017). The Ignateevo Formation dolomites formed under the shallow shelf conditions, with a reduced water exchange and anoxia, without significant terrigenous inflow.

CORRELATION OF THE IGNATEEVO FORMATION DOLOMITES AND CARBONATE DEPOSITS OF THE KAAPVAAL AND PILBARA CRATONS

The geological histories of the Kaapvaal, Pilbara, and Eastern Sarmatia cratons at the Archean–Paleoproterozoic boundary demonstrate many similarities; in this respect, it was supposed that, in the period of 2.8–2.2 Ga, Eastern Sarmatia was a part of the Vaalbara supercraton (Savko et al., 2017). In order to support (or reject) this hypothesis, we attempted to correlate carbonate deposits from these three cratons

according to their positions in sections, geochemical characteristics, and sedimentation conditions.

The best known Campbellrand–Malmani carbonate series is located within the limits of the Kaapvaal craton and occurs in the lower part of the Transvaal Supergroup; it accumulated at ~2.58–2.52 Ga (Sumner and Beukes, 2006). The Campbellrand–Malmani Platform is composed of dolomite stromatolites having different degrees of silicification, formed in shallow marine conditions. The Campbellrand series dolomites are underlain by sandy-carbonate deposits of the Schmidtsdrif Subgroup (Schröder et al., 2006) that unconformably superimpose metabasites of the Ventersdorp Supergroup (Fig. 6). Dolomites of the Malmani Dolomite occur on quartzites of the Black Reef Formation, which, in turn, unconformably occur on metabasites of the Ventersdorp Supergroup (Fig. 6). The Campbellrand–Malmani carbonate platform is unconformably superimposed by siliceous shales of the Klein Naute Formation and by thick ferriferous quartzites of the Kuruman and Penge formations with age of 2460 ± 5 Ma (Schröder et al., 2006). The appearance of shales and ferriferous quartzites reflects deepening of the basin in the Early Paleoproterozoic.

In addition, the Hamersley Basin (Pilbara craton) also hosts the Wittenoom–Carawine carbonate platform with age of 2.6–2.5 Ga (Jahn and Simonson, 1995; Nelson et al., 1999). The main lithologic difference between Wittenoom and Carawine dolomites is that the latter contain stromatolites, whereas they have not been found in the Wittenoom Dolomite (Simonson et al., 1993). The upper terrigenous part of the Wittenoom Dolomite comprises the Bee Gorge Member, above which the carboniferous shales of the Mount McRae Shale occur (Fig. 5). The Wittenoom Dolomite occur directly on metabasites of the Fortescue Group (2765–2687 Ma; Arndt et al., 1991). The Carawine Dolomite is underlain by the ferriferous Marra Mamba Iron Formation with age of 2597 ± 5 Ma (Simonson et al., 1993), occurring on metabasites of the Fortescue Group.

The existing correlations between the Kaapvaal and Pilbara cratons begin from 2.77 Ga and are based on paleomagnetic data and similarities between volcanogenic sections of the Fortescue and Ventersdorp groups (de Kock et al., 2009). Correlation of the sections and lithostratigraphic and paleogeographic reconstructions suggest that deposits in the lower part of the Transvaal Supergroup (namely, dolomites of the Campbellrand–Malmani Platform, Kuruman and Penge BIFs) and those of the Hamersley Supergroup (corresponding to the Wittenoom–Carawine carbonate platform and Brockman Iron Formation) formed in the united large partially closed oceanic basin in the margin of the ancient Vaalbara supercontinent (Beukes and Gutzmer, 2008).

The lower age limit of the Archean sedimentary sequence in Eastern Sarmatia is determined by the age of rhyolites comprising the Lebedinskaya Formation in the Tim-Yastrebovka structure, namely, 2610 ± 10 Ma (Savko et al., 2019). In the Mikhailovka structure, rocks of the Ignateevo Formation superimpose several complexes: metabasites of the Mikhailovka series (2.8–2.6 Ga in age), tonalite-trondhjemite gneisses of the Saltykovo complex (about 3 Ga), and gneiss-migmatites of the Oboyan complex (>3.2 Ga) (Figs. 1c, 2). The Neoarchean sedimentary sequence begins with polymictic conglomerates that change to metagravelites and metasandstones comformably superimposed by the Ignateevo Formation dolomites (Figs. 1c, 2). The Ignateevo Formation dolomites are in turn conformably overlain by terrigenous rocks of the Stoilo Formation represented by quartzite-like metasandstones and shales, sometimes carboniferous (Fig. 6). The Stoilo Formation is conformably overlain by the thick sequence of the Korobki BIF, whose structure coincides with that of the Kuruman BIF (Kaapvaal craton) and Brockman Iron Formation (Hamersley basin) up to the fine details (Savko et al., 2017).

Thus, we see the clear similarity between the sedimentary sections of the Kaapvaal, Pilbara, and Eastern Sarmatia cratons in the period of 2.6–2.4 Ga. Sedimentary sequences unconformably rest on Neoarchean metabasites of the Ventersdorp, Fortescue, and Mikhailovka series, respectively (Fig. 6). The sedimentary sequences of these three cratons begin with terrigenous deposits overlain by carbonate rocks (Campbellrand–Malmani and Wittenoom–Carawine platforms and Ignateevo Formation, respectively). The only exception is the Marra Mamba Iron Formation that divides terrigenous deposits of the Jeerinah Formation and Wittenoom carbonates in the Pilbara craton. Up the section, carbonate platforms of all cratons are superimposed by terrigenous siliceous and carboniferous rocks (Klein Naute Formation in the Kaapvaal craton, Bee Gorge Member and Mount McRae Shale in the Pilbara craton, and Stoilo Formation in Eastern Sarmatia). Finally, the sections of all cratons end with thick sequences of chemogenic ferriferous quartzites (Kuruman and Penge BIFs in the Kaapvaal craton, Brockman Iron Formation in the Pilbara craton, and Korobki BIF in Eastern Sarmatia).

Despite the tectonic proximity of the continental blocks of Sarmatia and Fennoscandia in the modern basement structure of the East European Platform, Early Precambrian terrigenous-carbonate sequences of the Kursk Block and the Ukrainian Shield differ from the coeval terrigenous-volcanogenic-carbonate sequence of the Baltic Shield. The Fennoscandian sections demonstrate no presence of ferriferous quartzites (Savko et al., 2017), while the age of carbonate sediments is younger than that of carbonate sediments of Sarmatia (Ovchinnikova et al., 2007; Kuznetsov et al., 2010, 2019).

Comparing further, we should note the similarity between epigenetic and metamorphic history of rocks

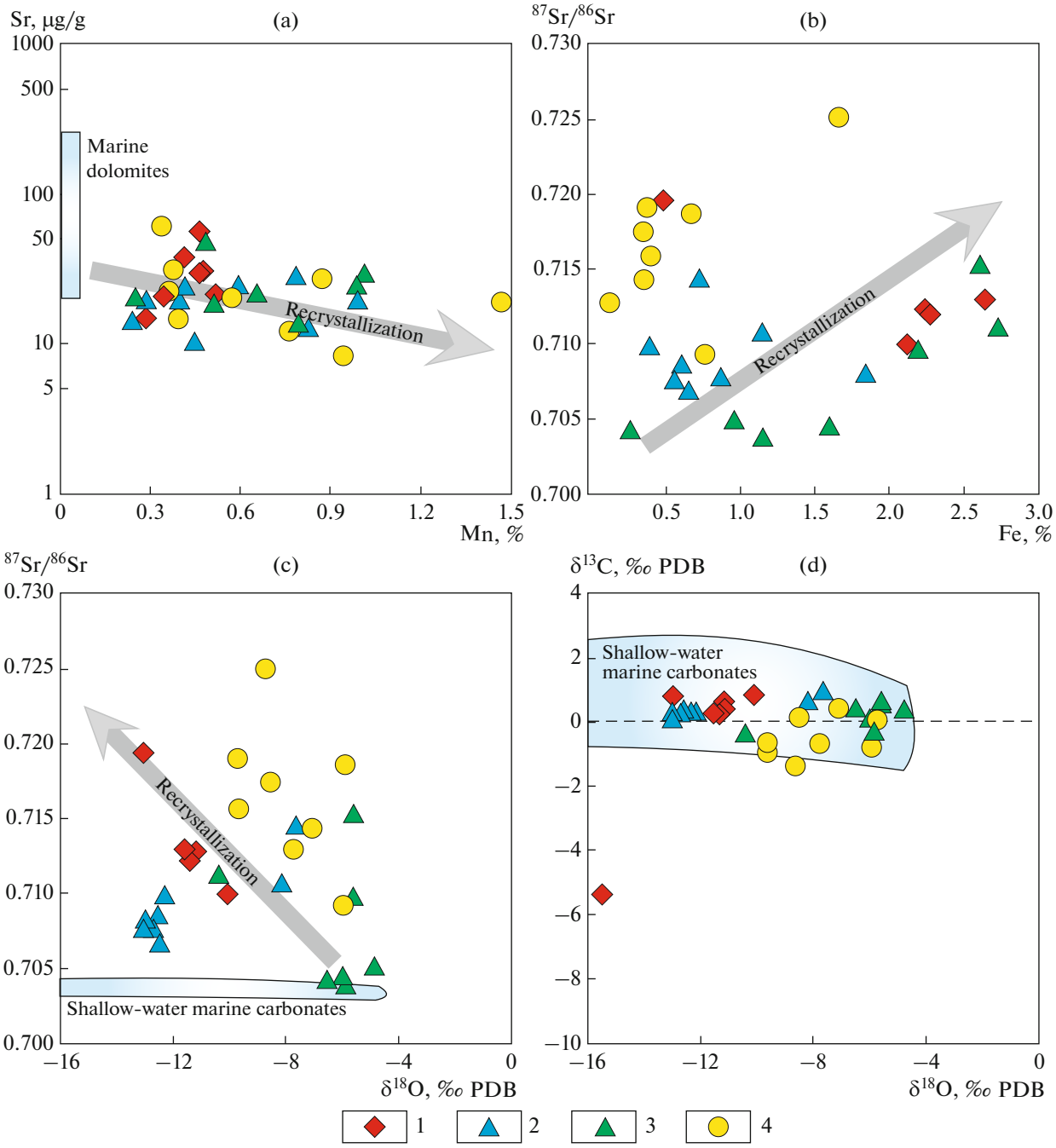

Fig. 5. Comparison between isotope-geochemical compositions of the Ignateevo Formation dolomites and Archean–Paleoproterozoic marine dolomites (Veizer et al., 1990; 1992; Kuznetsov et al., 2003, 2010, 2018). Blue domain corresponds to the zone of the least altered marine dolomites. Arrows mark the direction of epigenetic recrystallization. Legend: (1) dolomites, Ignateevo Formation, Kursk Block (present work); (2) Wittenoom Dolomite, Pilbara craton, Australia; (3) Carawine Dolomite, Pilbara craton, Australia; (4) Malmani Dolomite, Transvaal craton, South Africa.

in Eastern Sarmatia and those in the Kaapvaal and Pilbara cratons. Supracrustal sequences of Eastern Sarmatia underwent metamorphism and intense folding at 2.07 Ga. Carbonates of the Campbellrand–Malmani Platform also underwent thermal influence during the intrusion of the Bushveld igneous complex at 2.06 Ga. Despite this, dolomite structures are quite well-preserved, so that lithologic facies (tidal, shelf, lagoonal, and slope) can be distinguished, as well as stromatolite units (Sumner and Beukes, 2006).

Carbonate rocks of all three cratons are characterized by silicification and dolomitization, contain small amounts of silicoclastic material, and have low Sr con-

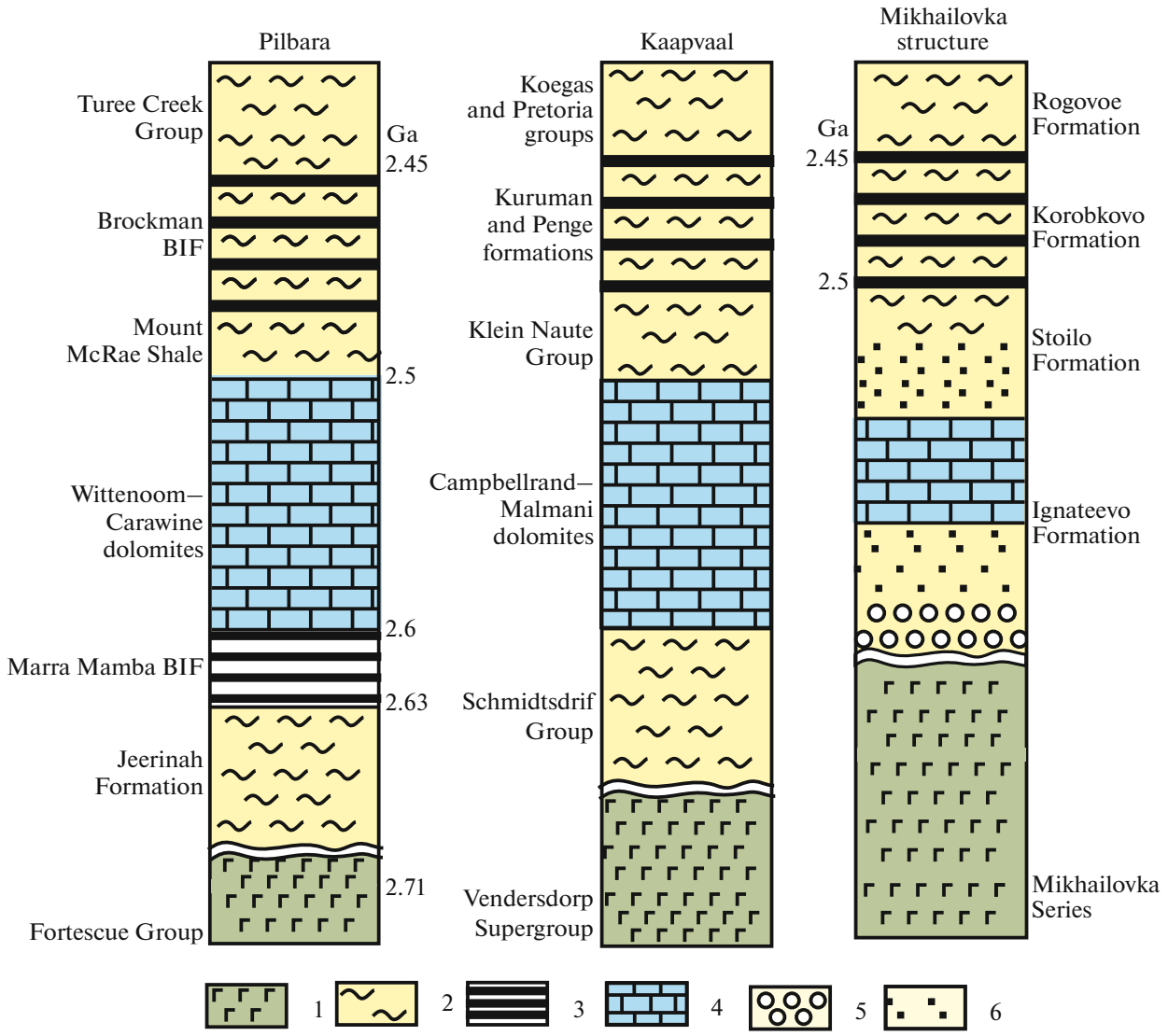

Fig. 6. Correlation scheme for the Neoarchean and Early Paleoproterozoic units from the Vaalbara basins, after (Beukes and Gutzmer, 2008; Nelson, 1999), and the Mikhailovka structure, Kursk Block of Sarmatia, after (Savko, 2017) with additions. Legend: (1) metabasites, (2) shales, (3) ferriferous quartzites, (4) carbonate rocks, (5) metaconglomerates, (6) terrigenous rocks.

centrations (Beukes, 1987; Veizer et al., 1990, 1992; Eroglu et al., 2015, 2017). Mean Sr contents are as follows: 18 μg/g in the Wittenoom Dolomite, 24 μg/g in the Carawine Dolomite, 27 μg/g in the Malmani Dolomite, and 31 μg/g in the Ignateevo Formation (Fig. 5). Dolomites of all three carbonate platforms are enriched in iron and manganese.

Dolomites of the Campbellrand–Malmani Platform, as well as carbonates of the Ignateevo Formation, revealed the REE distribution characteristic of Neoarchean paleooceans: low total concentrations, flat profiles on spider diagrams, positive La anomalies, absence of Ce anomaly, and Y/Ho ratios higher than the chondrite value (Bau and Dulski, 1996; Kamber and Webb, 2014; Eroglu et al., 2017; Franchi, 2018). Positive Eu anomalies can be noted in some specimens.

The values of $\delta^{13}C$ in the Ignateevo Formation dolomites and in the Wittenoom Dolomite fall within the range of 0.3–0.9‰ PDB (Fig. 5). The values of $\delta^{13}C$ in the Carawine and Malmani dolomites have close values, from –0.3 to 0.5‰ PDB and from –1.4 to 0.4‰ PDB, respectively. The $^{87}Sr/^{86}Sr$ ratio in the Ignateevo Formation dolomites (0.7101–0.7195) is close to that in the Malmani Dolomite (0.7093–0.7251), but higher than that in limestones of the Campbellrand Subgroup (0.7023–0.7050), in Wittenoom Dolomite (0.7067–0.7143), and in Carawine Dolomite (0.7037–0.7151) (Fig. 5). The minimum $^{87}Sr/^{86}Sr$ values of 0.7037 in the Carawine Dolomite (Veizer et al., 1990) and 0.7023–0.7038 in limestones of the Campbellrand Subgroup (Kamber and Webb, 2001) are characteristic of the Archean–Early Paleop-

roterozoic oceans (Kuznetsov et al., 2018). These values indicate the predominance of mantle Sr in oceans of that time and the absence of mature continental crust.

Thus, given the similarities between the sections of three cratons and close isotope-geochemical characteristics of carbonate rocks, we can assume that the respective sediments deposited in a united vast periodically shallowed oceanic basin. Most of the dolomites of the Campbellrand–Malmani Platform are of early diagenetic origin and formed as a result of dolomitization of limestones (Beukes, 1987). The least altered limestones were preserved in the margin of the Campbellrand carbonate platform, where circulation of oceanic waters was the most intense (Kamber and Webb, 2001). In the inner zones, where the Malmani Dolomite deposited, water circulation was less intense and water exchange with an open oceanic basin was less effective. This led to accumulation of Mg-rich solutions and dolomitization of carbonate deposits of the platform. It is this inner zone of the carbonate platform where the most widespread silicification took place. Rocks of the Malmani Dolomite were completely dolomitized and partially silicified (SiO_2 content is up to 86.7 wt %; Eroglu et al., 2015). Thus, in terms of geochemical characteristics, dolomites and calc-silicate rocks (intensely silicified dolomites) of the Ignateevo Formation are close to shallow marine dolomites of the Campbellrand–Malmani Platform. Probably, dolomites of the Ignateevo Formation and, to some degree, those of the Campbellrand–Malmani Platform formed in the most isolated part of the paleobasin, and this favored their complete dolomitization. Dolomites of the Wittenoom–Carawine Platform likely occurred at the periphery of the basin where better ocean water circulation took place, as a result of which partial dolomitization occurred and the initial stromatolitic limestones, whose analogs are absent in Eastern Sarmatia, were preserved.

CONCLUSIONS

The section of metasedimentary deposits of the Kursk Block, Eastern Sarmatia, has the terrigenous-carbonate deposits of the Ignateevo Formation at its bottom and includes BIFs characteristic of the Neoarchean and Paleoproterozoic. The Ignateevo Formation unconformably rests on Archean metabasites and on tonalite-trondhjemite and migmatite-gneissic complexes. The lower part of the Ignateevo Formation (110–680 m thick) is composed of polymictic conglomerates, gravelites, and sandstones, while the upper part is represented by dolomites up to 160 m thick. The Ignateevo Formation dolomites are overlain by terrigenous rocks of the Stoilo Formation, which in turn are superimposed by thick (more than 1 km) Korobki BIF.

The REE distribution in dolomites is characteristic of sediments in Neoarchean oceans: low total REE contents, flat profiles on spider diagrams, positive La anomalies, absence of Ce anomaly, and Y/Ho ratios higher than the chondrite value. The values of $\delta^{13}C$ (from 0.3 to 0.9‰ PDB) and $\delta^{18}O$ (from −10.1 to −13.0‰ PDB) fall within the narrow range characteristic of typical marine Neoarchean and Early Proterozoic carbonates. High values of the $^{87}Sr/^{86}Sr$ ratio (0.71014–0.71951) indicate recrystallization of dolomites and disturbance of their initial Rb–Sr isotope system, most likely as a result of metamorphism that occurred at 2.07 Ga. Very low concentrations of TiO_2, Al_2O_3, Na_2O, K_2O, Zr, Sc, and Th in dolomites suggest a minimal input of terrigenous material to the sedimentary paleobasin.

Dolomites of the Ignateevo Formation formed under the conditions of a shallow shelf in the passive continental margin, where reduced inflow of ocean water took place, providing the formation of Mg-rich solutions and early diagenetic dolomitization.

The similarity between sedimentary sequences of the Kaapvaal, Pilbara, and Eastern Sarmatia cratons for the period of 2.6–2.4 Ga, close isotope-geochemical characteristics of dolomites in carbonate platforms, and early diagenetic dolomitization and silicification are additional arguments for the common history of these units as parts of the united Vaalbara supercontinent.

FUNDING

Isotope studies were supported by the Russian Science Foundation (project. no. 18-17-00247).

Reviewers: I.M. Gorokhov, A.B. Kotov and A.V. Samsonov

REFERENCES

Allwood, A.C., Kamber, B.S., Walter, M.R., Burch, I.W., and Kanik, I., Trace elements record depositional history of an Early Archean stromatolitic carbonate platform, *Chem. Geol.*, 2010, vol. 270, pp. 148–163.

Arndt, N.T., Nelson, D.R., Compston, W., Trendall, A.F., and Thorne, A.M., The age of the Fortescue group Hamersley basin Western Australia from ion microprobe zircon U–Pb results, *Aust. J. Earth Sci.*, 1991, vol. 38, pp. 261–281.

Banner, J.L., Application of the trace-element and isotope geochemistry of strontium to studies of carbonate diagenesis, *Sedimentology*, 1995, vol. 42, pp. 805–824.

Bau, M. and Alexander, B., Preservation of primary REE patterns without Ce anomaly during dolomitization of Mid-Paleoproterozoic limestone and the potential reestablishment of marine anoxia immediately after the "Great Oxidation Event", *South African J. Geol.*, 2006, vol. 109, pp. 81–86.

Bau, M. and Dulski, P., Distribution of yttrium and rare-earth elements in the Penge and Kuruman iron-formations, Transvaal Supergroup, South Africa, *Precambrian Res.*, 1996, vol. 79, pp. 37–55.

Bekker, A., Chemostratigraphy of the Paleoproterozoic Duitschland Formation, South Africa: implications for coupled climate change and carbon cycling, *Am. J. Sci.*, 2001, vol. 301, pp. 261–285.

Beukes, N.J., Facies relations, depositional-environments and diagenesis in a major Early Proterozoic stromatolitic carbonate platform to basinal sequence, Campbellrand Subgroup, Transvaal Supergroup, Southern Africa, *Sediment. Geol.*, 1987, vol. 54, pp. 1–46.

Beukes, N.J. and Gutzmer, J., Origin and paleoenvironmental significance of major iron formations at the Archean–Paleoproterozoic boundary, *Soc. Econ. Geol. Rev.*, 2008, vol. 15, pp. 5–47.

Beukes, N.J., Klein, C., Kaufman, A.J., and Hayes, J.M., Carbonate petrography, kerogen distribution, and carbon and oxygen isotope variations in an Early Proterozoic transition from limestone to iron-formation deposition, Transvaal Supergroup, South Africa, *Econ. Geol.*, 1990, vol. 85, pp. 663–690.

Cheney, E.S., Sequence stratigraphy and plate tectonic significance of the Transvaal succession of Southern Africa and its equivalent in Western Australia, *Precambrian Res.*, 1996, vol. 79, pp. 3–24.

Condie, K.C., Chemical composition and evolution of the upper continental crust: contrasting results from surface samples and shales, *Chem. Geol.*, 1993, vol. 104, pp. 1–37.

Derry, L.A. and Jacobsen, S.B., The chemical evolution of Precambrian seawater – evidence from Rees Banded Iron Formations, *Geochim. Cosmochim. Acta*, 1990, vol. 54, pp. 2965–2977.

Eroglu, S., Schoenberg, R., Wille, M., Beukes, N., and Taubald, H., Geochemical stratigraphy, sedimentology, and Mo isotope systematics of the ca. 2.58–2.50 Ga-old Transvaal Supergroup carbonate platform, South Africa, *Precambrian Res.*, 2015, vol. 266, pp. 27–46.

Eroglu, S., van Zuilen, M.A., Taubald, H., Drost, K., Will, M., Swanner, E.D., Beukes, N.J., and Schoenberg, R., Depth-dependent $\delta^{13}C$ trends in platform and slope settings of the Campbellrand-Malmani carbonate platform and possible implications for Early Earth oxygenation, *Precambrian Res.*, 2017, vol. 302, pp. 122–139.

Franchi, F., Petrographic and geochemical characterization of the Lower Transvaal Supergroup stromatolitic dolostones (Kanye Basin, Botswana), *Precambrian Res.*, 2018, vol. 310, pp. 93–113.

Franchi, F., Hofmann, A., Cavalazzi, B., Wilson, A., and Barbieri, R., Differentiating marine vs hydrothermal processes in Devonian carbonate mounds using rare earth elements (Kess Kess mounds, Anti-Atlas, Morocco), *Chem. Geol.*, 2015, vol. 409, pp. 69–86.

Franchi, F., Rovere, M., Gamberi, F., Rashed, H., Vaselli, O., and Tassi, F., Authigenic minerals from the Paola Ridge (southern Tyrrhenian Sea): evidences of episodic methane seepage, *Mar. Petrol. Geol.*, 2017, vol. 86, pp. 228–247.

Frauenstein, F., Veizer, J., Beukes, N., Van Niekerk, H.S., and Coetzee, L.L., Transvaal Supergroup carbonates: implications for Paleoproterozoic $\delta^{18}O$ and $\delta^{13}C$ records, *Precambrian Res.*, 2009, vol. 175, pp. 149–160.

Gorbatschev, R. and Bogdanova, S., Frontiers in the Baltic shield, *Precambrian Res.*, 1993, vol. 64, pp. 3–21.

Gorokhov, I.M., Kuznetsov, A.B., Melezhik, V.A., Konstantinova, G.V., and Mel'nikov, N.N., Sr isotopic composition in the Upper Jatulian (Early Paleoproterozoic) dolomites of the Tulomozero Formation, Southeastern Karelia, *Dokl. Earth Sci.*, 1998, vol. 360, no. 4, pp. 609–612.

Gorokhov, I.M., Kuznetsov, A.B., Ovchinnikova, G.V., Nozhkin, A.D., Azimov, P.Ya., and Kaurova, O.K., Pb–Sr–O–C isotope compositions of metacarbonate rocks of the Derbina Formation (East Sayan): Chemostratigraphic and geochronological significance, *Stratigr. Geol. Correl.*, 2016, vol. 24, no. 1, pp. 1–18.

Hesse, R., Silica diagenesis: origin of inorganic and replacement cherts, *Earth-Sci. Rev.*, 1989, vol. 26, pp. 253–284.

Jahn, B. and Simonson, B.M., Carbonate Pb–Pb ages of the Wittenoom Formation and Carawine Dolomite, Hamersley Basin, Western Australia (with implications for their correlation with the Transvaal Dolomite of South Africa), *Precambrian Res.*, 1995, vol. 72, nos. 3–4, pp. 247–261.

Kamber, B.S. and Webb, G.E., The geochemistry of Late Archean microbial carbonate: implications for ocean chemistry and continental erosion history, *Geochim. Cosmochim. Acta*, 2001, vol. 65, pp. 2509–2525.

Kamber, B.S. and Webb, G.E., The rare earth element signal in Archaean microbial carbonate: information on ocean redox and biogenicity, *J. Geol. Soc. London*, 2014, vol. 171, pp. 745–763.

Klein, C. and Beukes, N.J., Geochemistry and sedimentology of a facies transition from limestone to iron-formation in the early Proterozoic Transvaal Supergroup, South Africa, *Econ. Geol.*, 1989, vol. 84, pp. 1733–1774.

Knauth, L.P., A model for the origin of chert in limestone, *Geology*, 1979, vol. 7, pp. 274–277.

de Kock, M.O., Evans, D.A.D., Kirschvink, J.L., Beukes, N.J., Rose, E., and Hilburn, I., Paleomagnetism of a Neoarchean-Paleoproterozoic carbonate ramp and carbonate platform succession (Transvaal Supergroup) from surface outcrop and drill core, Griqualand West region, South Africa, *Precambrian Res.*, 2009, vol. 169, pp. 80–99.

Van Kranendonk, M.J., Webb, G.E., and Kamber, B.S., New geological and trace element evidence from 3.45 Ga stromatolitic carbonates in the Pilbara Craton: support of a marine, biogenic origin and for a reducing Archaean ocean, *Geobiology*, 2003, vol. 1, pp. 91–108.

Kuznetsov, A.B., Melezhik, V.A., Gorokhov, I.M., Mel'nikov, N.N., and Fallick, E., Sr isotope composition in paleoproterozoic carbonates extremely enriched in C-13: Kaniapiskau Supergroup, the Labrador trough of the Canadian Shield, *Stratigr. Geol. Correl.*, 2003, vol. 11, no. 3, pp. 209–219.

Kuznetsov, A.B., Ovchinnikova, G.V., Krupenin, M.T., Gorokhov, I.M., Maslov, A.V., Kaurova, O.K., and Ellmies, R., Diagenesis of carbonate and siderite deposits of the Lower Riphean Bakal Formation, the Southern Urals: Sr isotopic characteristics and Pb–Pb Age, *Lithol. Miner. Resour.*, 2005, vol. 40, no. 3, pp. 195–215.

Kuznetsov, A.B., Semikhatov, M.A., and Gorokhov, I.M., Strontium isotope stratigraphy: Principles and state of the art, *Stratigr. Geol. Correl.*, 2018, vol. 26, no. 4, pp. 367–386.

Kuznetsov, A.B., Melezhik, V.A., Gorokhov, I.M., Melnikov, N.N., Konstantinova, G.V., Kutyavin, E.P., and Turchenko, T.L., Sr isotopic composition of Paleoproterozoic ^{13}C-rich carbonate rocks: the Tulomozero Formation, SE Fennoscandian Shield, *Precambrian Res.*, 2010, vol. 182, no. 4, pp. 300–312.

Kuznetsov, A.B., Lobach-Zhuchenko, S.B., Kaulina, T.V., and Konstantinova, G.V., Paleoproterozoic age of carbonates and trondhjemites of the Central Azov Group: Sr Iso-

tope chemostratigraphy and U–Pb geochronology, *Dokl. Earth Sci*., 2019, vol. 484, no. 2, pp. 142–145.

Leake, B.E. and Woolley, A.R., and 20 members of the Subcommittee on Amphiboles, Nomenclature of amphiboles. Report of the Subcommittee on Amphiboles of the International Mineralogical Association Commission on New Minerals and Mineral Names, *Eur. J. Mineral.*, 1997, vol. 9, pp. 623–651.

Maliva, R.G. and Siever, R., Nodular chert formation in carbonate rocks, *J. Geol.*, 1989, vol. 97, pp. 421–433.

McCrea, J.M., On the isotopic chemistry of carbonates and a paleotemperature scale, *J. Chem. Phys*., 1950, vol. 18, pp. 849–857.

Melezhik, V.A., Kuznetsov, A.B., Fallick, A.E., Smith, R.A., Gorokhov, I.M., Jamal, D., and Cataune, F., Depositional environments and an apparent age for the Geci meta-limestones: constraints on geological history of northern Mozambique, *Precambrian Res.*, 2006, vol. 148, nos. 1/2, pp. 19–31.

Melezhik, V.A., Kuznetsov, A.B., Pokrovsky, B.G., Solli, A., Gorokhov, I.M., Fallick, A.E., and Lindahl, I., Chemostratigraphic insight into deposition of the Melkedalen Marble formation, Narvik Nappe Complex, North-Central Norwegian Caledonides, *Norwegian J. Geol.*, 2014, vol. 93, pp. 35–50.

Melezhik, V.A., Ihlen, P.M., Kuznetsov, A.B., Gjelle, S., Solli, A., Gorokhov, I.M., Fallick, A.E., Sandstad, J.S., and Bjerkgård, T., Pre-Sturtian (800–730 Ma) depositional age of carbonates in sedimentary sequences hosting stratiform iron ores in the Uppermost Allochthon of the Norwegian Caledonides: a chemostratigraphic approach, *Precambrian Res*., 2015, vol. 261, pp. 272–299.

Nelson, D.R., Trendall, A.F., and Altermann, W., Chronological correlations between the Pilbara and Kaapvaal cratons, *Precambrian Res*., 1999, vol. 97, pp. 165–189.

Nozaki, Y., Zhang, J., and Amakawa, H., The fractionation between Y and Ho in the marine environment, *Earth Planet. Sci. Lett*., 1997, vol. 148, pp. 329–340.

Ovchinnikova, G.V., Kuznetsov, A.B., Melezhik, V.A., Gorokhov, I.M., Vasil'eva, I.M., and Gorokhovskii, B.M., Pb–Pb age of Jatulian carbonate rocks: The Tulomozero Formation of southeast Karelia, *Stratigr. Geol. Correl.*, 2007, vol. 15, no. 4, pp. 359–372.

Savko, K.A. and Poskryakova, M.V., Riebeckite-aegirine-celadonite BIF at the Mikhailovskoe Iron Deposit of the Kursk Magnetic Anomaly: phase equilibria and metamorphic conditions, *Petrology*, 2003a, vol. 11, no. 5, pp. 471-490.

Savko, K.A. and Poskryakova, M.V., Mineralogy, phase transformations, and metamorphism conditions of rocks of the Novoyaltinsk Iron Deposit of the Kursk Magnetic Anomaly, *Proceedings Voronezh State Univ., Ser. Geol.*, 2003b, no. 2, pp. 113–130.

Savko, K.A., Bazikov, N.S., and Artemenko, G.V., Geochemical evolution of the banded iron formations of the Voronezh Crystalline Massif in the early Precambrian: Sources of matter and geochronological constraints, *Stratigr. Geol. Correl.*, 2015, vol. 23, no. 5, pp. 451–467.

Savko, K.A., Samsonov, A.V., Kholin, V.M., and Bazikov, N.S., The Sarmatia megablock as a fragment of the Vaalbara supercontinent: Correlation of geological events at the Archean–Paleoproterozoic transition, *Stratigr. Geol. Correl.*, 2017, vol. 25, no. 2, pp. 123–145.

Savko, K.A., Samsonov, A.V., Kotov, A.B., Sal'nikova, E.B., Korish, E.H., Larionov, A.N., Anisimova, I.V., and Bazikov, N.S., The Early Precambrian metamorphic events in Eastern Sarmatia, *Precambrian Res.*, 2018a, vol. 311, pp. 1–23.

Savko, K.A., Samsonov, A.V., Larionov, A.N., Korish, E.Kh., and Bazikov, N.S., An Archaean tonalite–trondhjemite–granodiorite Association of the Kursk Block (Voronezh Massif): composition, age, and correlation with the Ukrainian Shield, *Dokl. Earth Sci*., 2018b, vol. 478, no. 1, pp. 115–119.

Savko, K.A., Samsonov, A.V., Kholina, N.V., Larionov, A.N., Zaitseva, M.V., Korish, E.H., Bazikov, N.S., and Terentiev, R.A., 2.6 Ga high-Si rhyolites and granites in the Kursk Domain, Eastern Sarmatia: petrology and application for the Archaean palaeocontinental correlations, *Precambrian Res*., 2019, vol. 322, pp. 170–192.

Schröder, S., Lacassie, J.P., and Beukes, N., Stratigraphic and geochemical framework of the Agouron drill cores, Transvaal Supergroup (Neoarchean–Paleoproterozoic, South Africa), *South African J. Geol*., 2006, vol. 109, pp. 23–54.

Simonson, B.M., Shubel, K.A., and Hassler, S.W., Carbonate sedimentology of the early Precambrian Hamersley Group of Western Australia, *Precambrian Res*., 1993, vol. 60, pp. 287–335.

Sumner, D. and Beukes, N., Sequence stratigraphic development of the Neoarchean Transvaal carbonate platform, Kaapvaal Craton, South Africa, *South African J. Geol*., 2006, vol. 109, pp. 11–22.

Tang, L., Santosh, M., Tsunogae, T., and Maruoka, T., Paleoproterozoic meta-carbonates from the central segment of the Trans-North China Orogen: zircon U–Pb geochronology, geochemistry, and carbon and oxygen isotopes, *Precambrian Res*., 2016, vol. 284, pp. 14–29.

Tucker, M. and Wright, V.P., *Carbonate Sedimentology*, Oxford: Blackwell Sci. Publ., 1990.

Veizer, J., Clayton, R.N., Hinton, R.W., von Brunn, V., Mason, T.R., Buck, S.G., and Hoefs, J., Geochemistry of Precambrian carbonates: III. Shelf seas and non-marine environments of the Archean, *Geochim. Cosmochim. Acta*, 1990, vol. 54, no. 10, pp. 2717–2729.

Veizer, J., Clayton, R.N., and Hinton, R.W., Geochemistry of Precambrian carbonates: IV. Early Paleoproterozoic (2.25 + 0.25) seawater, *Geochim. Cosmochim. Acta*, 1992, vol. 56, no. 3, pp. 875–885.

Warren, J., Dolomite: occurrence, evolution and economically important associations, *Earth Sci. Rev*., 2000, vol. 52, pp. 1–81.

Zhang, K.-J., Li, Q.-H., Yana, L.-L., Zeng, L., Lua, L., Zhang, Y.-X., Hui, J., Jin, X., and Tang, X.-C., Geochemistry of limestones deposited in various plate tectonic settings, *Earth Sci. Rev*., 2017, vol. 167, pp. 1–21.

Zhong, S. and Mucci, A., Partitioning of rare earth elements (REEs) between calcite and seawater solutions at 25°C and 1 atm, and high dissolved REE concentrations, *Geochim. Cosmochim. Acta*, 1995, vol. 59, pp. 443–453.

Translated by N. Astafiev